

**BATTERY MANAGEMENT SYSTEM FOR  
AUTOMATED GUIDED VEHICLE**

**LEONG QI YE**

**UNIVERSITI TUNKU ABDUL RAHMAN**

**BATTERY MANAGEMENT SYSTEM FOR  
AUTOMATED GUIDED VEHICLE**

**LEONG QI YE**

**A project report submitted in partial fulfilment of the  
requirements for the award of Bachelor of Mechatronics  
Engineering with Honours**

**Lee Kong Chian Faculty of Engineering and Science  
Universiti Tunku Abdul Rahman**

**October 2023**

**DECLARATION**

I hereby declare that this project report is based on my original work except for citations and quotations which have been duly acknowledged. I also declare that it has not been previously and concurrently submitted for any other degree or award at UTAR or other institutions.

Signature :   
\_\_\_\_\_

Name : Leong Qi Ye  
\_\_\_\_\_


ID No. : 19UEB06395  
\_\_\_\_\_

Date : 6 October 2023  
\_\_\_\_\_

**APPROVAL FOR SUBMISSION**


I certify that this project report entitled “**BATTERY MANAGEMENT SYSTEM FOR AUTOMATED GUIDED VEHICLE**” was prepared by **LEONG QI YE** has met the required standard for submission in partial fulfilment of the requirements for the award of Bachelor of Mechatronics Engineering with Honours at Universiti Tunku Abdul Rahman.

Approved by,

Signature :  \_\_\_\_\_

Supervisor : Dr. Hau Lee Cheun  
\_\_\_\_\_

Date : 6 October 2023  
\_\_\_\_\_

Signature :  \_\_\_\_\_

Co-Supervisor : Ir. Dr. Danny Ng Wee Kiat  
\_\_\_\_\_

Date : 7/10/23  
\_\_\_\_\_

The copyright of this report belongs to the author under the terms of the copyright Act 1987 as qualified by Intellectual Property Policy of Universiti Tunku Abdul Rahman. Due acknowledgement shall always be made of the use of any material contained in, or derived from, this report.

© 2023, LEONG QI YE. All right reserved.

## ACKNOWLEDGEMENTS

I would like to thank everyone who had contributed to the successful completion of this project. I would like to express my gratitude to my research supervisors, Dr. Hau Lee Cheun and Ir. Dr. Danny Ng Wee Kiat for their invaluable advice, guidance and enormous patience throughout the development of the research.

In addition, I would also like to express my gratitude to my loving parents and friends who had helped and given me encouragement to complete this project.

## ABSTRACT

While substantial research efforts have been devoted to optimizing various aspects of automated guided vehicles (AGVs), such as localization, path planning, and object recognition, there has been a relative lack of information concerning battery pack power management for AGVs. It is important to acknowledge that the performance and lifespan of batteries are significantly influenced by their charging and discharging patterns. Going beyond the recommended upper voltage limit during charging can trigger thermal runaway, potentially leading to battery destruction. Conversely, discharging batteries below the specified lower voltage limit can result in reduced capacity, thereby affecting overall battery performance. Therefore, a battery management system (BMS) was developed for AGVs in this Final Year Project (FYP) to provide essential functions such as charge and discharge current measurements, battery pack voltage measurement, and state of charge (SoC) estimation using the coulomb counting method. The developed BMS underwent rigorous testing on an AGV within UTAR to validate its performance. Experimental tests, including the accuracy of current sensing, battery pack voltage sensing, and SoC estimation during charging and discharging, demonstrated that the BMS effectively monitors the electrical characteristics, thus, providing insights for adequate usage and management of the AGV's battery pack. Key features of the developed BMS include SoC estimation, crucial for accurately assessing remaining battery capacity, and integration with the Internet of Things (IoT) for real-time data collection and storage during battery charging and discharging. This data holds immense value as it can be leveraged for analysis and future research in areas such as preventive maintenance, safety operating envelopes, and assessments related to the remaining useful life of the battery.

## TABLE OF CONTENTS

<b>DECLARATION</b>		<b>i</b>
<b>APPROVAL FOR SUBMISSION</b>		<b>ii</b>
<b>ACKNOWLEDGEMENTS</b>		<b>iv</b>
<b>ABSTRACT</b>		<b>v</b>
<b>TABLE OF CONTENTS</b>		<b>vi</b>
<b>LIST OF TABLES</b>		<b>viii</b>
<b>LIST OF FIGURES</b>		<b>ix</b>
<b>LIST OF SYMBOLS / ABBREVIATIONS</b>		<b>xii</b>
<b>LIST OF APPENDICES</b>		<b>xiii</b>
<b>CHAPTER</b>		
<b>1</b>	<b>INTRODUCTION</b>	<b>1</b>
1.1	General Introduction	1
1.2	Importance of the Study	1
1.3	Problem Statement	2
1.4	Aim and Objectives	3
1.5	Scope and Limitation of the Study	3
1.6	Contribution of the Study	4
1.7	Outline of the Report	5
<b>2</b>	<b>LITERATURE REVIEW</b>	<b>6</b>
2.1	Introduction	6
2.2	Overview of Battery Management System	7
2.3	Summary	15
<b>3</b>	<b>METHODOLOGY AND WORK PLAN</b>	<b>16</b>
3.1	Introduction	16
3.2	Battery Selection and Early Preparation	16
3.3	Mechanical Design of the Battery Pack	17
3.4	Electrical Design of Battery Management System	19
3.5	Percentage Error Calculation	26



3.6	Schematic Diagram of the Battery Management System	26
3.7	Flowchart of the Battery Management System Prototype	29
3.8	Data Recording	29
3.9	Cost of Building the Battery Management System	30
3.10	Gantt Chart	30
3.11	Summary	31
<b>4</b>	<b>RESULTS AND DISCUSSION</b>	<b>32</b>
4.1	Introduction	32
4.2	Hardware Implementation	32
4.3	Software Implementation	38
4.4	Implementation Issues and Challenges	39
4.5	System Evaluation and Discussion	42
4.6	Summary	49
<b>5</b>	<b>CONCLUSIONS AND RECOMMENDATIONS</b>	<b>50</b>
5.1	Conclusions	50
5.2	Recommendations for Future Work	51
	<b>REFERENCES</b>	<b>54</b>
	<b>APPENDICES</b>	<b>56</b>

**LIST OF TABLES**

Table 3.1:	The BOM list and the Total Price for One Unit of Battery Management System.	30
Table 4.1:	The Discharging Current and the Respective Voltage	44
Table 4.2:	The Trials of Voltage Measurement using Multi-meter and Voltage Sensor	48

## LIST OF FIGURES

Figure 1.1:	The Bloated Battery Pack due to Overcharged.	4
Figure 2.1:	The Basic Block Diagram of BMS (Spoorthi and Pradeepa, 2022)	7
Figure 2.2:	The Overview of the Battery Management System (Liu, Placke and Chau, 2022).	8
Figure 2.3:	The Battery Pack Topologies Commonly Used (Lelie et al., 2018)	11
Figure 2.4:	Example Circuit of Active Cell Balancing Circuit (Arendarik and Radhoštem, 2012)	12
Figure 2.5:	Example Circuit of Passive Cell Balancing Circuit (Scott and Nork, 2023).	12
Figure 3.1:	The 18650 Batteries That Would be Used.	17
Figure 3.2:	The Spot-welding Machine and the Lithium-ion Batteries being Spot Welded (WinAck, 2023).	17
Figure 3.3:	The Lithium-ion Battery Pack Design using SolidWorks.	18
Figure 3.4:	Block Diagram of the Electronic Component	19
Figure 3.5:	The Typical Application Circuit of the INA169 (Texas Instrument, 2017).	20
Figure 3.6:	The Shunt Resistance and Their Respective Current Sense Range Extracted from Hymel (2023).	21
Figure 3.7:	The Illustration of the Voltage Divider Rule.	22
Figure 3.8:	The ADC vs Voltage Input to the ADC Pin (Espressif, 2023).	23
Figure 3.9:	The Smart DALY BMS that will be used.	24
Figure 3.10:	The Alternate 7S BMS Without Communication.	25
Figure 3.11:	The ESP32S3 Devkit being Implemented.	26
Figure 3.12:	The Schematics Diagram of the Battery Management System Prototype.	27

Figure 3.13:	The Charge and Discharge Control and Current Sensing Schematics Diagram.	28
Figure 3.14:	The Schematics Diagram of the prototype	28
Figure 3.15:	The Flowchart of the Control of the Battery Management System.	29
Figure 3.16:	The Gantt Chart of FYP1.	31
Figure 3.17:	The Gantt Chart of FYP.	31
Figure 4.1:	The 7S Lithium Battery Pack with Smart Daly BMS.	33
Figure 4.2:	The Mobile Phone App of the Daly BMS.	34
Figure 4.3:	The Assembled 7S Lithium-ion Battery Pack with Another BMS.	35
Figure 4.4:	The Disassembled 7S Lithium-ion Battery Pack.	35
Figure 4.5:	The Hardware of the Battery Management System Prototype.	36
Figure 4.6:	The INA169 Shunt Current Monitor Module being Implemented.	37
Figure 4.7:	The Voltage Sensor of the Battery Management System.	37
Figure 4.8:	The Double Channel Relay Module.	38
Figure 4.9:	The DC-DC Buck Converter being Implemented.	38
Figure 4.10:	The GUI of the Daly BMS during Charging Current Around One Ampere.	40
Figure 4.11:	The Charging Current Output by the Charger.	40
Figure 4.12:	The Actual Resistance of R1 and R2 Measured.	42
Figure 4.13:	The Discharging Current and Voltage Across Shunt Resistor.	43
Figure 4.14:	The Discharging Current and Voltage Across Shunt Resistor.	43
Figure 4.15:	The Voltage Measured by the Voltage Sensor (Trial 1).	45
Figure 4.16:	The Voltage Measured by the Multi-meter (Trial 1).	45

Figure 4.17: The Voltage Measured by the Voltage Sensor (Trial 2).	46
Figure 4.18: The Voltage Measured by the Multi-meter (Trial 2).	46
Figure 4.19: The Voltage Measured by the Voltage Sensor (Trial 3).	47
Figure 4.20: The Voltage Measured by the Multi-meter (Trial 3).	47
Figure 4.21: The SOC and Pack Voltage Versus Time Curve.	48
Figure 4.22: Discharging and Charging Voltage and SOC of the Battery Pack.	49

**LIST OF SYMBOLS / ABBREVIATIONS**

$\Omega$	Resistance, ohm ( $\Omega$ )
ADC	Analog-to-Digital Converter
AGV	Automated Guided Vehicle
BMS	Battery Management System
CAD	Computer Aided Design
FYP	Final Year Project
IC	Integrated Circuit
IOT	Internet of Things
MQTT	Message Queuing Telemetry Transport
RF	Radiofrequency
SoC	State of Charge
SoH	State of Health

**LIST OF APPENDICES**

Appendix A:	The Code of the Battery Management System Prototype (main).	57
Appendix B:	The Subfile of the Code (relay_control_h)	59
Appendix C:	The Subfile of the Code (relay_control.cpp)	59
Appendix D:	The Subfile of the Code (current_sensing_h)	60
Appendix E:	The Subfile of the Code (current_sensing.cpp)	60
Appendix F:	Datasheet of INA169 Shunt Current Monitor	62
Appendix G:	The Drawing of Battery Casing (Top Bracket)	63
Appendix H:	The Drawing of Battery Casing (Bottom Bracket)	63
Appendix I:	The Drawing of battery Casing (8S Bracket but can Fit 7S also)	64

## CHAPTER 1

### INTRODUCTION

#### 1.1 General Introduction

In the context of the impending Industrial Revolution 4.0, the adoption of automated guided vehicles (AGVs) within the industrial landscape has substantially substituted human involvement, particularly in tasks characterized by heavy loads and repetitive operations, such as warehouse management.

As indicated by Lynch et al., (2018), various categories of AGVs are presently employed within manufacturing facilities, encompassing forklifts, unit load vehicles, pallet trucks, and towing vehicles. Despite their diverse functionalities, these AGVs uniformly rely on electric power for their operation. Notably, they depart from traditional machines tethered to lengthy electrical cords, as AGVs are furnished with rechargeable battery systems, ensuring a consistent supply of electrical energy.

To uphold the operational integrity of these AGVs, the rechargeable battery system necessitates an efficient framework that operates within a controlled and secure environment. Such a setup serves as an assurance of the peak performance of automated guided vehicles.

#### 1.2 Importance of the Study

The rechargeable battery pack is a consumable component of AGVs. Unfortunately, it is often neglected, with people assuming that any charger can be used to recharge the battery, or the battery can be used for any load so long it meets the voltage requirement. However, this neglect has significant consequences, leading to battery bloating and a drastically reduced lifespan.

The battery management system (BMS) for rechargeable battery pack plays a crucial role in extending their lifespan. This system not only safeguards the battery with onboard protective devices and battery balancer, but it also monitors the batteries' electrical characteristics, such as charging and discharging currents, battery pack voltage, state of charge (SoC), and state



of health (SoH). This data empowers users to plan AGV usage more effectively. For instance, having knowledge of battery's SOC allows AGV users to optimize the workloads by selectively charging and tasking specific AGVs in the factory, resulting in maximum benefits of knowing the available capacity remaining in the batteries.

Moreover, ensuring a reliable power source for AGVs is vital to prevent injuries to personnel working with them due to power source uncertainties. A robust battery pack system with BMS also safeguards electrical components like DC motors, robotic arm, sensors and onboard controllers from damage resulting from battery failure. In case of an abnormal battery pack condition such as overload, the BMS would immediately cut off the supply to protect other components or systems on the AGV.

Furthermore, there is potential for enhancing AGV energy efficiency. For instance, when the BMS of the battery pack system balances cell charge levels, it prolongs the battery pack's lifespan compared to systems without BMS. The longevity of the AGV's battery system can also be further improved by installing appropriate battery management software. This prevents the frequent replacement of battery cells due to adverse operating conditions. An effective BMS ensures that individual battery cells conform to the manufacturer's established life cycle.

In short, this study contributes to reducing AGV development costs. Without a proper BMS, a significant portion of the budget must be allocated for frequent battery replacements. However, having a reliable BMS, it would significantly reduce the power system costs in the development and maintenance of AGV.

### **1.3 Problem Statement**

In the context of this Final Year Project (FYP), particularly on the current scenario of AGV development in UTAR, the problem statement are as follows: UTAR is currently engaged in the study and development of various AGVs for ROBOCON and home assistance-related research. Regrettably, the AGVs employed within UTAR lack a well-structured BMS. Consequently, the lithium polymer (LiPo) battery utilized to power these AGVs exhibits a short

lifespan and necessitates frequent replacement, e.g., two to three times a year and each LiPo cost around RM 80 to RM 100. Consequently, the primary objective of this project is to design a BMS aimed at rectifying this issue.

#### **1.4 Aim and Objectives**

This project aims to develop a BMS to monitor the battery parameters and control its supply in the charging-discharging facets of AGV. In particular, those designed and developed in UTAR. The objectives of this project are, thus, as follows:

1. To identify the current, voltage, and other interfacing electronics needed for the BMS development with a budget of RM 500.
2. To develop a BMS prototype for AGV's battery pack within 25-week timeframe.
3. To validate the performance of the BMS in term of charging and discharging the battery pack.

#### **1.5 Scope and Limitation of the Study**

The primary scope of this FYP is to design and develop a BMS for AGV's battery pack to govern its inflow and outflow of currents/powers within the desired safety operating envelop. It is important to note that this project would not delve into an extensive investigation of advanced algorithms, such as machine learning-based SOC estimation for the battery pack. Furthermore, the primary emphasis of this project is on the embedded system and electrical aspect of the BMS, with less detailed attention to the mechanical design of the battery pack.

However, it is important to acknowledge certain limitations of this study. Firstly, there is a time constraint, with the FYP expected to be completed within a 25-week timeframe. Consequently, time management is crucial to ensure the successful achievement of the project's aim and objectives. Additionally, this project faces budget limitations, with only RM 500 allocated for the FYP. As a result, careful consideration and comparison of electronic components are essential before making any purchases to make the most of the limited funds available.

## 1.6 Contribution of the Study

The implementation of a proper BMS holds paramount importance as it significantly extends the lifespan of battery pack. Without a proper BMS, batteries are susceptible to accidental damage. Within the UTAR robotics society, many students employ rechargeable battery pack like LiPo to test their AGVs, often without the necessary protective measures available in BMS.

In this context, any mishandling of the battery can lead to defects. A recent incident serves as a pertinent example, where a student accidentally overcharged the battery due to incorrect settings on the battery charger. As a consequence, the overcharging rendered the battery irreparably damaged, causing it to bloat, such as illustrated in Figure 1.1.

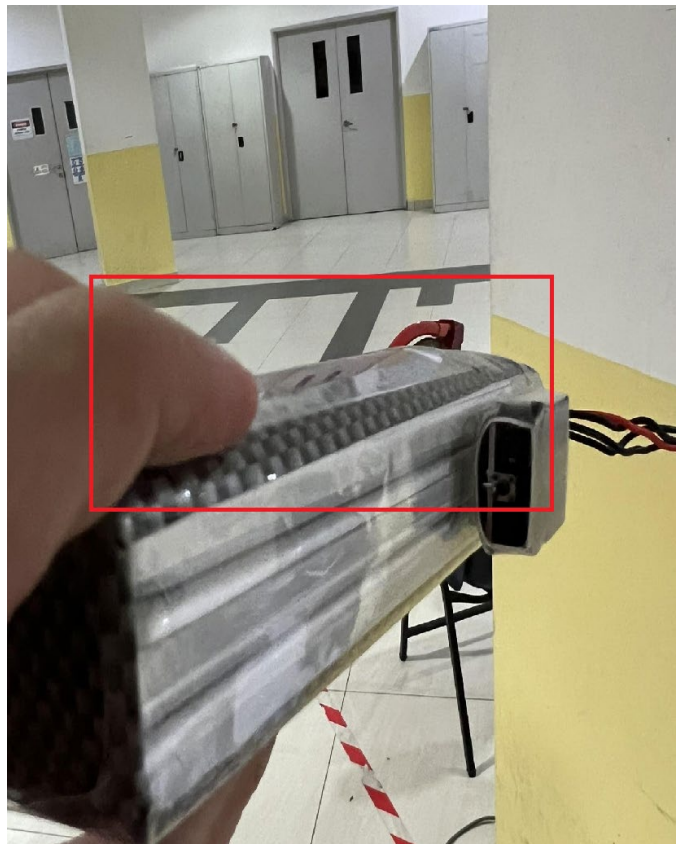


Figure 1.1: The Bloated Battery Pack due to Overcharged.

This hazardous condition significantly shortens the battery's lifespan compared to other batteries from the same batch. In essence, such accidents impose an additional financial burden on students developing their AGVs.

Therefore, on the local level, the development and implementation of a BMS would greatly benefit UTAR students by safeguarding their batteries and preventing such incidents from impacting their projects.

### **1.7 Outline of the Report**

This report is divided into five chapters. The first chapter encompasses the general introduction, problem statement, aims and objectives of the project, as well as an outline of the FYP's scope and limitations. Chapter 2 delves into the literature review, focusing on BMS methodology and providing an overview of the components within and its frameworks. Chapter 3 outlines the methodology employed in developing the BMS, while Chapter 4 presents the results and discussions stemming from the development of the developed BMS. Finally, Chapter 5 encapsulates the project's conclusion and its implications as well as offers recommendations for future work.

## CHAPTER 2

### LITERATURE REVIEW

#### 2.1 Introduction

BMS has the capability to estimate essential parameters such as SoC and state of health (SoH) of the battery, provided there is sufficient data, including charging and discharging currents, and battery cells' voltages. Subsequently, the values derived for SoC and SoH can be transmitted to the user through a communication interface, allowing real-time monitoring of the battery's status.

Furthermore, BMS requires a well-designed control algorithm capable of processing data collected by sensors such as the current sensor, which measures charging and discharging currents, and the voltage sensor, responsible for monitoring pack voltage. Once processed, the communication interface facilitates the transmission of this data from the BMS to the end user.

Figure 2.1 shows the block diagram of a BMS, showing the crucial link between the battery pack and the components underlying it namely, the measurement, the state estimations, the thermal management, and cell balancing. Each of these components will be elaborated in this chapter.

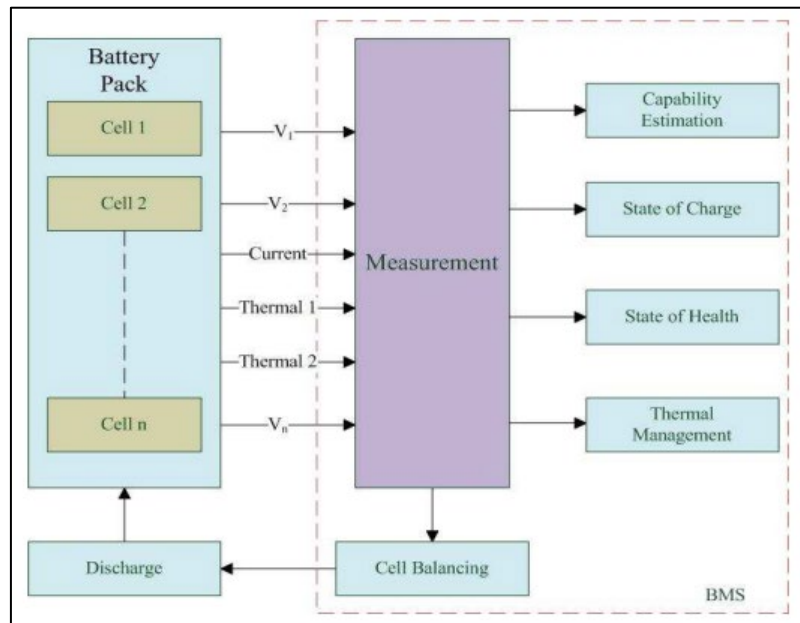


Figure 2.1: The Basic Block Diagram of BMS (Spoorthi and Pradeepa, 2022)

## 2.2 Overview of Battery Management System

Li et al., (2018) have emphasized that a comprehensive BMS should encompass critical functions, including thermal management, state of charge estimation, cell monitoring, and cell balancing. Expanding on this, Wang et al. (2020) have identified additional essential functions, such as fault diagnosis, discharge and charge control, as well as communication with external devices.

To realize these multifaceted functions, various hardware components, including sensors, safety circuits, and microcontrollers, must be integrated into the BMS. Figure 2.2 provides an overview of the battery management system, illustrating its essential components and their interconnections.

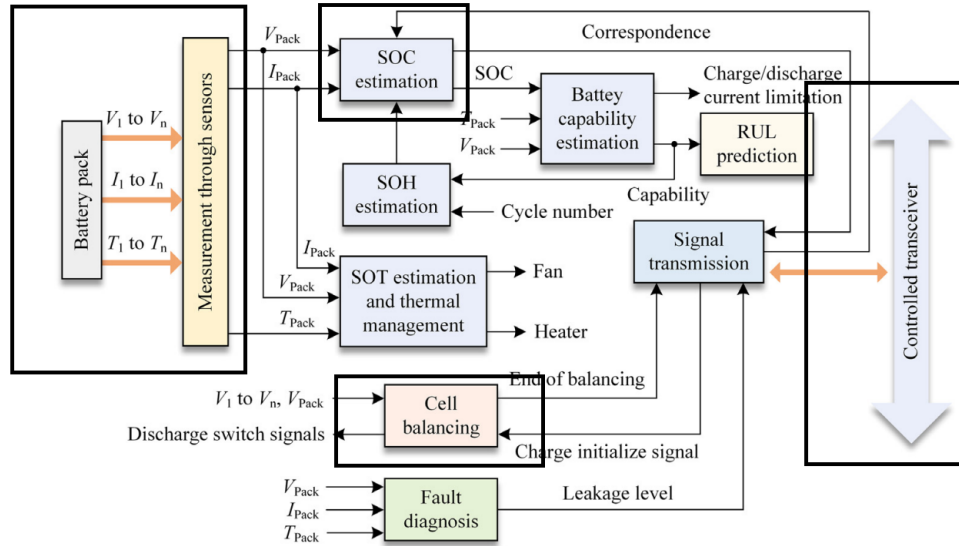


Figure 2.2: The Overview of the Battery Management System (Liu, Placke and Chau, 2022).

To establish a basic BMS, it is imperative to achieve the components highlighted within the black solid boxes in Figure 2.2. Firstly, a sensor system must be in place to continuously monitor the battery pack. These sensors gather critical data related to the battery's state and performance. Secondly, the data obtained from these sensors should be processed to estimate the SoC of the battery pack. This calculation is pivotal for tracking the battery's energy levels accurately.

Next, a transceiver is essential to facilitate communication of this vital information to the end user via various communication protocols. This real-time data transmission ensures the user is well-informed about the battery's status and can take appropriate actions. Lastly, the cell balancing circuit serves a crucial role by ensuring the equalization of charge among individual cells within the battery pack. This function promotes uniform cell performance and extends the overall lifespan of the battery pack.

### 2.2.1 Sensor and Measurement System

Gathering information about the battery pack is of utmost importance for the BMS as it enables the BMS to be informed about the batteries' states and protect it before any breakdowns. Consequently, various types of sensors are

required to measure crucial parameters of the battery pack, such as temperature, current, and voltage.

These sensors are critical because they directly impact the BMS's performance. As highlighted in the research paper by Lelie et al. (2018), the accuracy of voltage sensing plays a pivotal role in the performance of SoC estimation for the battery pack. In a BMS proposed by Ceven et al. (2021), the authors implemented operational amplifiers in differential mode. This configuration allows the microcontroller to capture individual cell voltages within the battery pack. This measurement technique involves connecting the positive terminal of each adjacent battery cell to the operational amplifier. The output of the amplifier is then read by the microcontroller. However, this method of cell voltage measurement consumes multiple pins of the microcontroller equipped with analog-to-digital conversion (ADC) functionality to read the voltage levels of each battery cell in the pack. The authors mentioned using the OPA4197 operational amplifier, which integrates four channels into a single integrated circuit (IC), facilitating a more compact design.

On the other hand, Lakkireddy and Mathe (2022) incorporated optocouplers in their BMS design to measure individual cell voltages. The PC817 optocoupler was used, comprising an LED and photodiode pair. The authors initially employed a voltage divider circuit to scale down the battery cell voltage to a safe range for the optocoupler's operation. And on the output side of the optocoupler, a pull-up resistor was implemented on the collector pin to provide a reference voltage for the microcontroller's ADC pin. The emitter of the optocoupler was connected to ground, and when the LED emitted light, activating the photodiode, the voltage read by the microcontroller's ADC pin changed accordingly. This working principle allowed for the measurement of each cell voltage in a systematic yet safe manner.

Furthermore, Lakkireddy and Mathe also employed the WCS1800 current sensor to monitor the battery pack's current. The WCS1800, which utilizes the Hall effect (Winson, 2020), measures current without the need for direct physical connection to the battery pack. Instead, a wire from the battery



pack passes through the sensor, providing electrical isolation to the microcontroller.

Conversely, in the BMS proposed by Nizam et al. (2019), the authors employed the MAX471 current sensor IC (Maxim Integrated, n.d.) to measure current. The MAX471 measures current through a shunt resistor, which is a low-value and precise resistor connected across the battery pack's output. Using Ohm's law, the voltage across the resistor is proportional to the current, with the resistance known. Therefore, the measured voltage provides information about the current magnitude.

In short, individual cell voltages can be measured using voltage divider circuits or operational amplifiers, with the latter offering superior sensing capabilities but necessitating compensation for offset voltage. Meanwhile, monitoring the current flow into and out of a battery pack can be achieved through hall effect sensors or shunt resistors, with the latter method susceptible to noise issues at low current levels.

### **2.2.2 Cell Voltage Measurement Circuit**

In reference to Figure 2.3, the configuration marked as (b) represents two cells connected in parallel to create a single-cell module. On the other hand, configuration (d) involves parallel connections of two strings of series cells to form a battery pack. Additionally, configuration (e) creates a battery pack by connecting the cell modules in series, as described for (b).

For this project, the individual voltages of each battery cell within the pack are crucial for further processing by the microcontroller's algorithm. In alignment with Figure 2.3, this project has adopted topology (c). As noted in the referenced research in Section 2.2.1, monitoring voltage channels is necessary. However, in this project, the battery pack consists of seven individual cells connected in series. Consequently, the microcontroller must monitor all seven voltage channels during operation to accurately obtain the cell voltages.

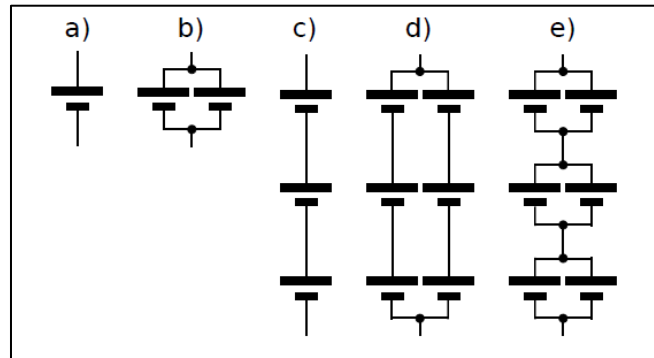


Figure 2.3: The Battery Pack Topologies Commonly Used (Lelie et al., 2018)

### 2.2.3 Cell Balancing System

In the battery pack, battery cells are arranged and connected in series to achieve the desired voltage value. The electrical characteristics of these cells may exhibit slight variations due to differences in the chemical composition resulting from the manufacturing process (Xing et al., 2011). Consequently, the actual capacity of each battery cell can vary. Cells with lower capacity will charge more rapidly than those with higher capacity, leading to voltage imbalances during the charging and discharging of the battery pack.

According to Cao, Schofield, and Emadi (2008), there are two primary methods for addressing the cell imbalance within a battery pack over the passive or the active means. The key distinction between these methods lies in how they manage the energy transfer between cells. Active cell balancing transfers excess electrical energy to cells that are not fully charged. In contrast, passive cell balancing dissipates surplus electrical energy through resistors, converting it into heat energy.

Comparatively, active cell balancing is more efficient, minimizing energy losses during the balancing process. However, passive cell balancing offers a simpler implementation, as its circuit design is relatively less complex compared to active cell balancing circuits, which rely on intricate pathways for electron flow between cells (Omariba, Zhang and Sun, 2019). Figure 2.5 and 2.6 shows the example circuit of an active and passive balancers, respectively.

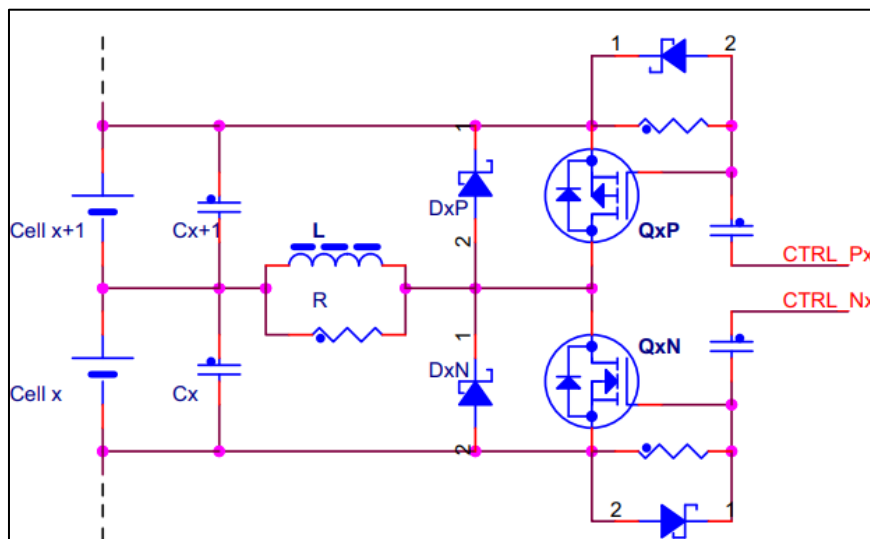


Figure 2.4: Example Circuit of Active Cell Balancing Circuit (Arendarik and Radhoštem, 2012)

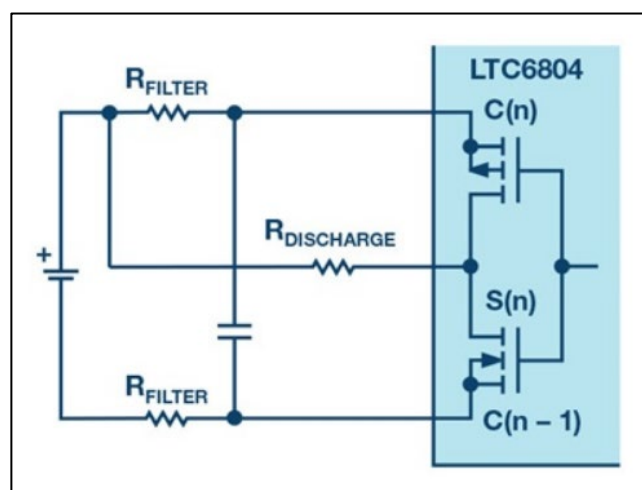


Figure 2.5: Example Circuit of Passive Cell Balancing Circuit (Scott and Nork, 2023).

## 2.2.4 Control Algorithm

In the operation of BMS, the control algorithm embedded within the microcontroller of a BMS plays a pivotal role. This algorithm relies on data acquired from sensors integrated into the BMS, processing this information, and subsequently instructing system responses. An exemplary scenario highlighting its significance is the control of battery charging and discharging, which directly impacts both the safety and efficiency of the battery pack. By employing a well-designed control algorithm within the microcontroller,

undesirable events such as overcharging and over discharging can be effectively averted (Wang and Yin, 2021).

Furthermore, the control algorithm encompasses SoC estimation for the battery pack. It dictates appropriate responses to be executed on the battery pack based on its SoC. For instance, the algorithm can be programmed to halt the discharging process when the SoC falls below a user-defined threshold. In this FYP, SoC estimation is achieved using the Coulomb counting method, contributing to precise monitoring and control.

### **2.2.5 State of Charge Estimation**

In a review by (Shete et al., n.d.), SoC estimation methods are categorized into three primary types: Book-Keeping Estimation, Model-Based, and Direct Measurement. The latter two categories, Model-Based and Direct Measurement, encompass various specific techniques. Notably, the Book-Keeping method corresponds to the Coulomb counting method.

Coulomb counting is a technique employed to determine the remaining capacity of the battery pack, commonly referred to as SoC. It serves as a valuable indicator for users regarding the remaining charge in the battery. This method involves tracking the flow of current into and out of the battery pack during its operation, utilizing a current sensor. The accuracy of SoC estimation through Coulomb counting depends on both the battery's capacity and the initial SoC of the battery pack. Nevertheless, it is essential to acknowledge a limitation of this method where the accuracy of current measurements obtained from the sensor directly impacts the SoC estimation since it relies entirely on precise current measurements during battery operation (Movassagh et al., 2021).

### **2.2.6 Microcontroller**

The microcontroller serves as a critical component within the BMS, essentially functioning as its central processing unit. The selection of an appropriate microcontroller is essential, as it must possess features tailored to support the BMS's operations. The market offers a diverse array of microcontrollers suitable for building a BMS.

In a BMS proposed by Akarslan and Çinar (2022), the chosen microcontroller is the STM32 from STMicroelectronics. This microcontroller is responsible for executing various tasks, including managing sampling intervals for analog signals originating from current, voltage, and temperature sensors, controlling resistor balancing, initiating and concluding charge and discharge phases, and facilitating data transfer through the user interface.

Moreover, there are plans by the authors to incorporate the BMS algorithm currently running on the interface directly into the microcontroller's firmware, enabling real-time execution without complications. The STM32 microcontroller was chosen due to its substantial processing capacity, energy efficiency, and a rich assortment of peripherals, such as ADCs and communication interfaces. These factors significantly influenced the decision-making process. Additionally, the STM32 microcontroller benefits from comprehensive development tools and software support, simplifying the creation and deployment of the BMS.

Conversely, in the BMS developed by Ceven et al. (2021), an Arduino Nano microcontroller is employed. In their BMS, the microcontroller's role is to gather data and oversee BMS operations, including monitoring temperature, cell voltages, and current. Subsequently, the data collected is transmitted to the primary controller, an ESP32, via radio frequency (RF) communication. This configuration allows the BMS to function as part of an Internet of Things (IoT) system. The Message Queuing Telemetry Transport (MQTT) protocol is utilized for implementing IoT capabilities, enabling the transfer of gathered battery data to an online environment. During the charging process, the MQTT server can instruct the network to adjust voltage levels for each node as needed. Thus, IoT functionality facilitates data transmission from the BMS to an online environment for monitoring and control purposes.

Furthermore, several electronics design companies have developed their own ICs tailored for battery monitoring, including Texas Instruments in the United States. Texas Instruments' battery monitor ICs offer crucial features necessary for a comprehensive BMS. For instance, in a reference design by Texas Instrument (2016), a battery management module supporting up to 20

battery cells in series is presented. The battery monitoring IC, BQ76930, is capable of cell parameter measurement, battery balancing, and protection functions. This IC can seamlessly communicate with a microcontroller, also from Texas Instruments, via the I2C communication protocol. Consequently, the microcontroller is relieved of the need to execute extensive control algorithms, as the dedicated battery monitoring IC efficiently handles many essential BMS functions.

In short, the choice of microcontroller in a BMS depends on the specific requirements and capabilities needed for the system, with various options available to cater to different design objectives and goals.

### **2.3 Summary**

Based on the literature review in this chapter, it is essential to prioritize the implementation of sensors with a streamlined and compact design within the BMS to make the most of limited project space like the one in this FYP. Therefore, opting for voltage measurement through divider circuit is used due to requirement of an offset voltage for operational amplifiers. Regarding current sensing, a combination of shunt resistors and current sense ICs should be incorporated into the design. This choice is made because, compared to hall effect sensors, it allows for a reduction in the circuit's height, a crucial consideration for size-constrained projects. For cell balancing, a passive cell balancing approach is the preferred choice. This method offers a less intricate circuit design and, most importantly, is cost-effective compared to active cell balancers. Furthermore, the ESP32 microcontroller is an ideal choice for this application. The ESP32 is an open-source microcontroller readily available in the market at a reasonable price. Its open-source nature provides a wide range of implementation options within the BMS design, ensuring flexibility and adaptability.

## CHAPTER 3

### METHODOLOGY AND WORK PLAN

#### 3.1 Introduction

The development of a BMS holds the potential to significantly enhance the performance of the AGV while also prolonging the lifespan of the battery pack. As mentioned in Chapter 1, historical experiences within the robotics society in UTAR have underscored the importance of adequate protection for rechargeable battery pack like LiPo. Without proper safeguards, the battery pack can deteriorate rapidly, leading to issues such as bloating, which can compromise the robot's functionality. Hence, this FYP has been initiated to address the challenges posed by inadequately protected batteries. Furthermore, a well-implemented battery protection system not only ensures the longevity of batteries but can also result in cost savings during robotics competitions where batteries are frequently utilized.

In this context, the scenario in UTAR is as follows where there is an ongoing project involving the development of an AGV by a FYP student. The student's design allocates a specific space with dimensions of 30cm x 15cm x 20cm for the battery pack system. Consequently, the mechanical design of the BMS with battery pack must adhere to the size constraints, ensuring seamless integration with the existing AGV framework. This chapter in hope to bring to light the development of the BMS from conceptual design to prototype.

#### 3.2 Battery Selection and Early Preparation

Figure 3.1 shows the chosen rechargeable batteries for this FYP; the 18650 lithium-ion batteries. It is imperative that all 18650 lithium-ion batteries undergo a full charging cycle before integration into the battery pack. This precaution is necessary due to potential variations in the batteries' chemistry. Failure to fully charge the batteries in unison may result in disparate initial states of charge, primarily stemming from losses incurred during shipping or storage, as outlined by Bhatt et al. (2017).



Figure 3.1: The 18650 Batteries That Would be Used.

### 3.3 Mechanical Design of the Battery Pack

Lithium-ion battery packs available in the market are typically assembled using a spot-welding process, such as shown in Figure 3.2, where a spot welder is used to join the lithium-ion battery cells together. Nickel strips serve as the connecting medium between these cells, facilitating their assembly. However, it's important to note that this method of joining battery cells together requires ensuring that the battery cells are in good condition before spot welding. If there are any design changes or if any of the battery cells are found to be defective, the process of replacing the defective cell can be time-consuming.

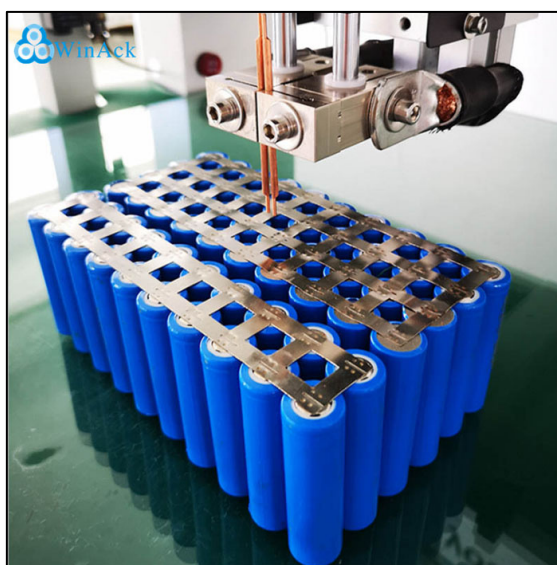


Figure 3.2: The Spot-welding Machine and the Lithium-ion Batteries being Spot Welded (WinAck, 2023).



Therefore, after conducting research and drawing inspiration from the design presented by Maloney (2018), an alternative, more flexible method for assembling lithium-ion battery cells has been identified. As shown in Figure 3.3, this method involves creating a suitable casing with pre-installed nickel strips in specially designed slots, which are configured to form a series connection of seven cells.

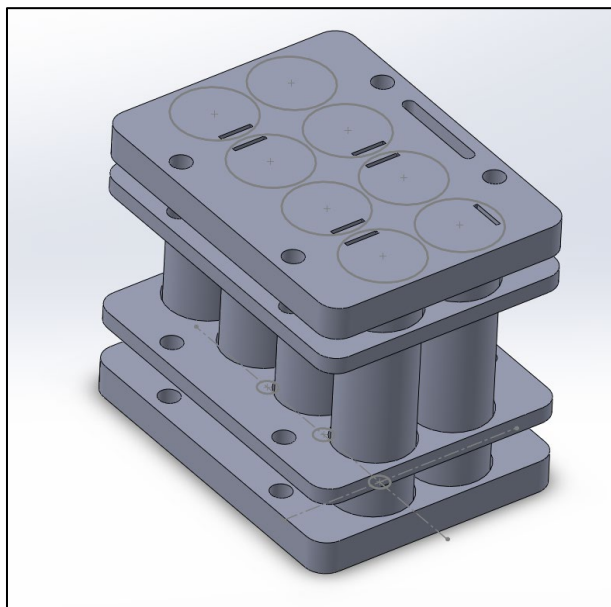


Figure 3.3: The Lithium-ion Battery Pack Design using SolidWorks.

Following the assembly of the battery cells and nickel strips within the casing, the enclosure is securely fastened using bolts. In the proposed design, the conventional nuts have been replaced with brass inserts. This modification allows for a robust tightening force generated by the bolts and brass inserts, ensuring a consistent and reliable connection between the battery cells. With this design, the process of replacing any individual cell becomes straightforward. All that is required is to disassemble the battery pack by removing the bolts, replace the necessary cells, and then re-tighten the bolts to reassemble the pack.

The mechanical Computer-Aided Design (CAD) design of the battery pack was completed using SolidWorks software. While the original design mentioned by the author in Maloney (2018) employed acrylic material for the casing, which necessitated the use of equipment like laser cutters to shape the

casing, this FYP opted for a different approach to expedite prototyping and reduce costs. Specifically, 3D printing is chosen as the source of fabrication method for the casing, offering a more efficient and cost-effective means of production.

### 3.4 Electrical Design of Battery Management System

The development of BMS prototype is contingent upon the careful selection of electronic components to ensure the functionality of the BMS. As highlighted in Chapter 2, a BMS serves several essential functions and incorporates various features to optimize the performance and safety of a battery pack. These functions and features encompass tasks such as monitoring individual cell voltages and temperatures, controlling charge and discharge processes, implementing cell balancing, and safeguarding against overcharging and over-discharging. Figure 3.4 provides a visual representation of the block diagram of the proposed BMS, showcasing the crucial components and their interconnections, which collectively contribute to achieving these functions and features.

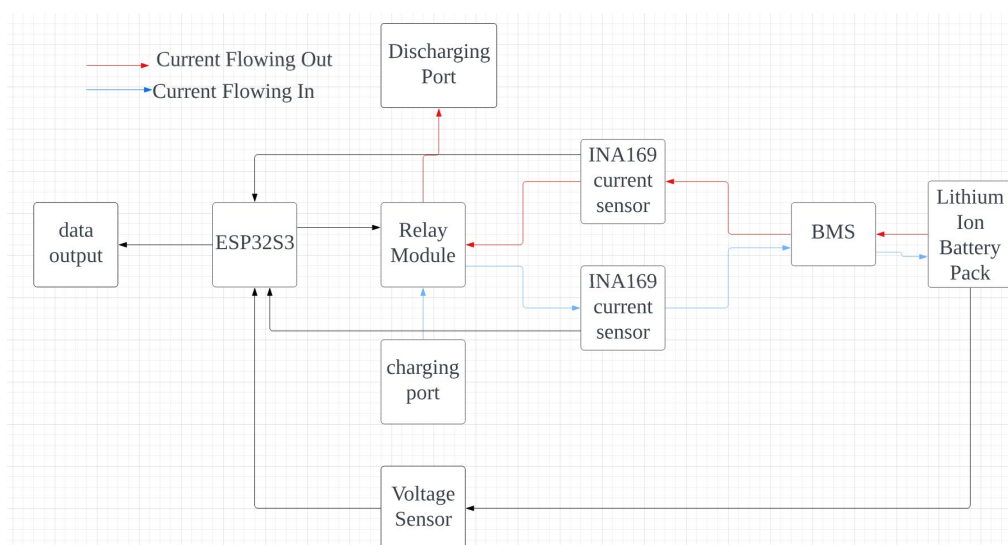


Figure 3.4: Block Diagram of the Electronic Component

#### 3.4.1 Current Measurement

In this FYP, the current measurement within the BMS is achieved by incorporating a current sensor called the INA169 high-side current shunt

monitor, manufactured by Texas Instruments. The application circuit diagram of the sensor is as shown in Figure 3.5. The transfer function of the INA169 based on the datasheet is given in Equation (3.1). The sensor was integrated into the BMS to accurately measure both the discharge and charge currents of the lithium-ion battery pack.

$$V_{OUT} = I_S R_S (1000 \mu A/V) R_L \quad (3.1)$$

Where,

$I_S$  = The current flow through the shunt resistor

$R_S$  = The shunt resistance

$R_L$  = The load resistor

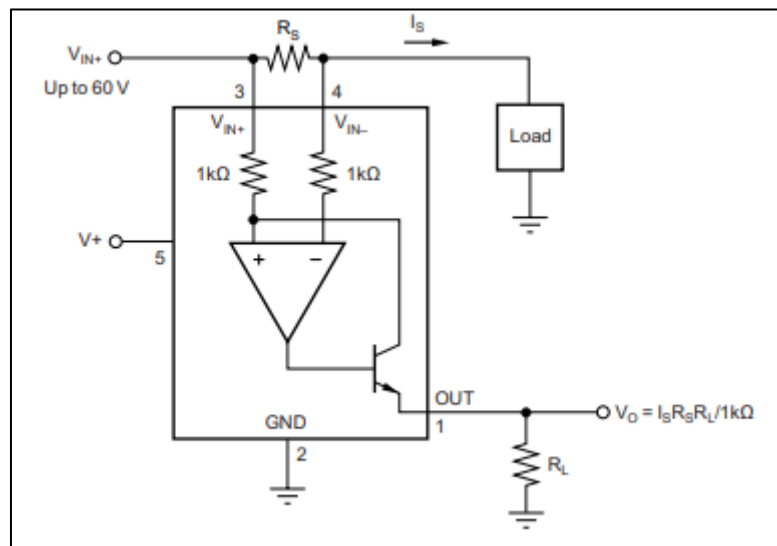


Figure 3.5: The Typical Application Circuit of the INA169 (Texas Instrument, 2017).

The functionality of the shunt monitor relies on the presence of a shunt resistor, which allows the integrated circuit to measure the differential voltage across the resistor. Subsequently, the output from the integrated circuit is measured by the ADC pin of the microcontroller to gauge the voltage. Applying Ohm's law, the current passing through the shunt resistor can then be calculated.

To expedite the development process and save time, rather than constructing the shunt current monitoring circuit from scratch, a pre-made INA169 module available in the market was procured. However, this module required some modifications to align with the specific requirements of the BMS design.

Initially, the module was equipped with a  $10\Omega$  shunt resistor, resulting in a limited current range spanning from 3.5mA to 35mA as shown in Figure 3.6. Recognizing this limitation and leveraging available resources, the  $10\Omega$  shunt resistor was replaced with a  $0.5\Omega$  high-power resistor, effectively addressing this issue and expanding the current measurement capabilities of the BMS.

$R_S$	Current Sense Range
$10\Omega$	3.5mA - 35mA
$1\Omega$	35mA - 350mA
$0.1\Omega$	350mA - 3.5A

Figure 3.6: The Shunt Resistance and Their Respective Current Sense Range  
Extracted from Hymel (2023).

Since the INA169 module comes pre-installed with a  $10k\Omega$  load resistor. Substituting this value into Equation (3.1), would result the voltage gain at the output to 10 times the voltage across the shunt resistor, denoted as ISRs. Assuming the maximum current passing through the shunt resistor is 2A, the voltage at the output of the INA169 would be calculated as  $2A \times 0.5\Omega \times 10$ , which equals 10V. However, it is important to note that the ADC pin of the microcontroller in use can only sample voltages up to 3.3V. Consequently, the load resistor needed to be replaced.

To simplify the algorithm within the microcontroller and ensure that the voltage does not exceed the ADC's range, the load resistance was replaced with a  $1k\Omega$  resistor. As a result, the voltage gain was reduced to 1, allowing for accurate voltage measurements within the ADC's 3.3V limit.

### 3.4.2 Voltage Measurement

In this FYP, the voltage measurement in the BMS is achieved through a voltage divider circuit as shown in Figure 3.7. The maximum voltage of an individual 18650 lithium-ion battery is 4.2V. When seven batteries are connected in series, the string voltage can reach a maximum combined voltage of 29.4V. However, it's important to note that the ADC pin of the microcontroller used in this BMS; ESP32S3 Devkit, has a limited voltage sampling range.

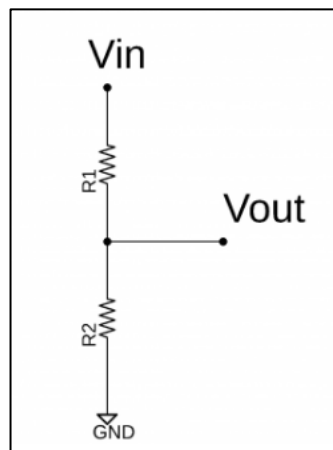


Figure 3.7: The Illustration of the Voltage Divider Rule.

According to the ESP32S3 ADC manual, the voltage range that can be accurately sampled by the microcontroller should not exceed 3.23V. Figure 3.8 shows the ADC value of the ESP32 will saturate if the voltage input exceeds 2805mV. Therefore, it is necessary to reduce the maximum voltage of the battery pack, which is 29.4V, to a voltage level that falls within the ADC's sampling range and avoids saturation.

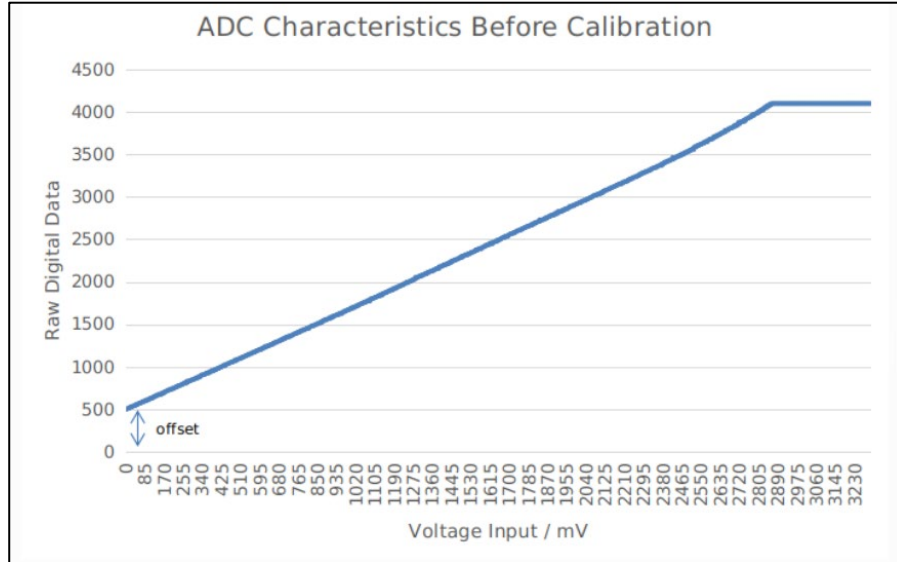


Figure 3.8: The ADC vs Voltage Input to the ADC Pin (Espressif, 2023).

Applying the Voltage Divider Rule, as expressed in Equation (3.2), and considering the available resources, the resistance values chosen for resistors R1 and R2 are 100k $\Omega$  and 10k $\Omega$ , respectively. It is important to note that resistors may have slight tolerances, leading to variations in their actual resistance values. To ensure accurate voltage measurements, the actual resistance values of the resistors should be measured and incorporated into the microcontroller's algorithm. This adjustment accounts for any discrepancies in the resistor values, ensuring precise voltage readings in the BMS.

$$V_{OUT} = \frac{R_2}{R_1 + R_2} V_{IN} \quad (3.2)$$

Where,

$V_{OUT}$  = Output Voltage, V

$R_1$  = Resistance of the first resistor,  $\Omega$

$R_2$  = Resistance of the second resistor,  $\Omega$

$V_{IN}$  = Input Voltage, V

### 3.4.3 Daly Battery Management System

The Daly BMS is a commercial BMS that offers communication capabilities. This BMS operates as a common port BMS, meaning that the charging and

discharging functions share the same port. To charge the battery, users must remove the battery pack and connect the charger to the port typically used for discharge. Figure 3.9 provides an illustration of the Daly BMS along with its Bluetooth module.

The Daly BMS in question is designed for a 7S lithium-ion battery configuration and offers key features like Bluetooth and UART (Universal Asynchronous Receiver-Transmitter) communication. When the Bluetooth module is connected to the BMS, it enables the transmission of various information, including SoC, charging, or discharging current, total battery pack voltage, individual battery cell voltages, and the status of charging and discharging MOSFETs.

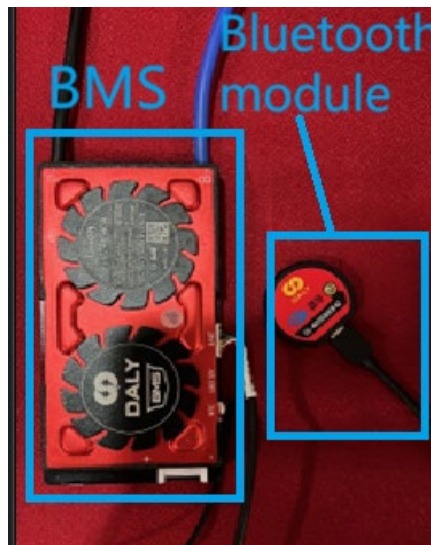


Figure 3.9: The Smart DALY BMS that will be used.

Within the community, there exists an open-source Daly BMS library that allows users to harness the UART port of the Daly BMS for data retrieval. However, it is important to note that the UART port is shared with the Bluetooth module, meaning that only one of these communication methods can be utilized at any given time.

During the development process, there was an issue with the functionality of the Daly BMS, which necessitated its replacement with an alternative 7S BMS lacking communication capabilities, as depicted in Figure

3.10. Same as the Daly BMS, this alternative BMS also operates as a common port BMS.



Figure 3.10: The Alternate 7S BMS Without Communication.

#### 3.4.4 Microcontroller

Figure 3.11 shows the picture of a ESP32S3 microcontroller that was chosen as the central component for the battery management system prototype. The rationale behind selecting this microcontroller is its powerful Central Processing Unit (CPU), which consists of a dual-core 32-bit microprocessor capable of operating at speeds of up to 240MHz.

Furthermore, the microcontroller is compatible with the open-source Arduino Integrated Development Environment (IDE), which facilitates the programming process. The availability of an open-source IDE means there is a wide array of resources and references accessible for software implementation, making development more convenient and versatile.



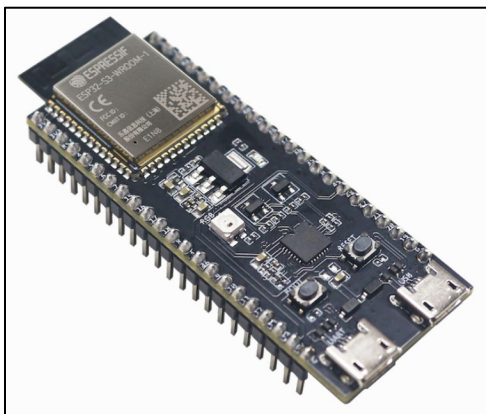


Figure 3.11: The ESP32S3 Devkit being Implemented.

### 3.5 Percentage Error Calculation

The percentage error of the results should be calculated with the following equation:

$$\text{percentage error, \%} = \left| \frac{\text{measured value} - \text{calculated value}}{\text{calculated value}} \right| \times 100\% \quad (4.1)$$

### 3.6 Schematic Diagram of the Battery Management System

The schematic diagram of the BMS was meticulously crafted using Autodesk Eagle, a CAD software renowned for its capabilities in electronic design. Following the completion of the schematics, the prototype will be constructed in accordance with the diagram's specifications. Figure 3.12 provides an encompassing view of the BMS prototype's schematic diagram, offering a comprehensive visualization of the system's layout and components.

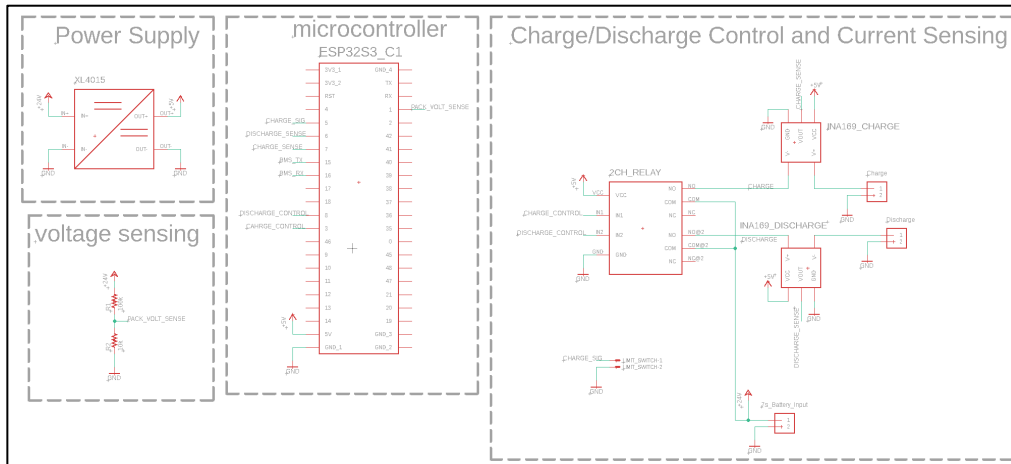


Figure 3.12: The Schematics Diagram of the Battery Management System Prototype.

Figure 3.13 presents the charge and discharge control as well as the current sensing circuit of the prototype. Notably, a noteworthy feature to highlight is that the charging control signal of the prototype is achieved by shorting the jumper together with the ground connection. This unique design element allows for precise and straightforward control over the charging process. Figure 3.14 then illustrates the schematic diagram, encompassing components and connections not previously covered in Figure 3.12. This diagram provides a complementary view of the additional circuitry and elements that are integral to the overall BMS prototype.

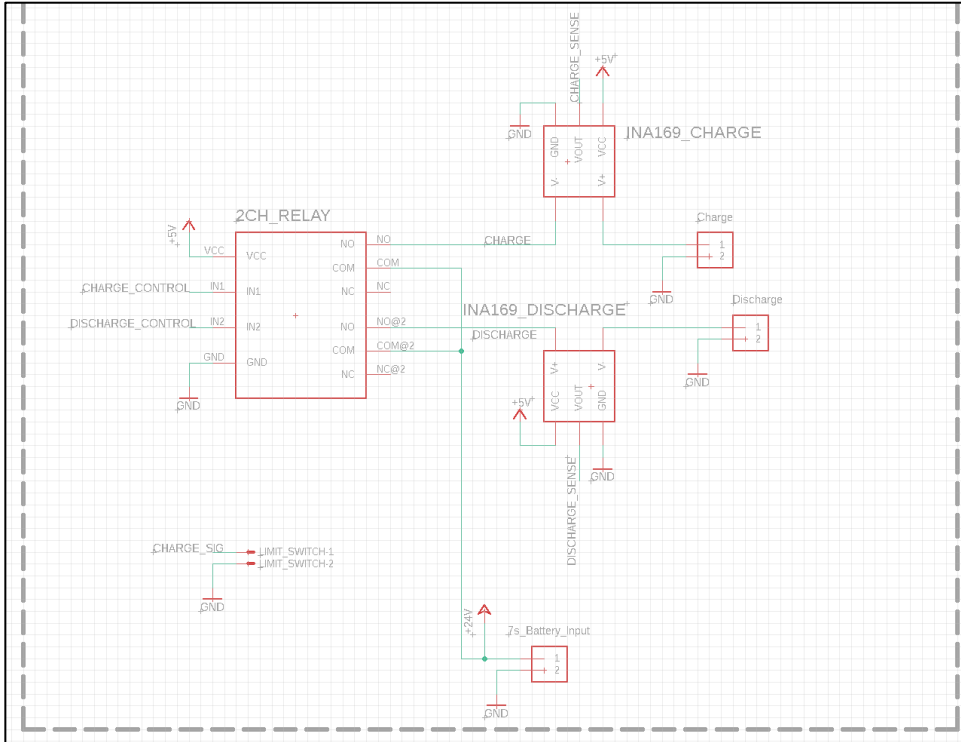


Figure 3.13: The Charge and Discharge Control and Current Sensing Schematics Diagram.

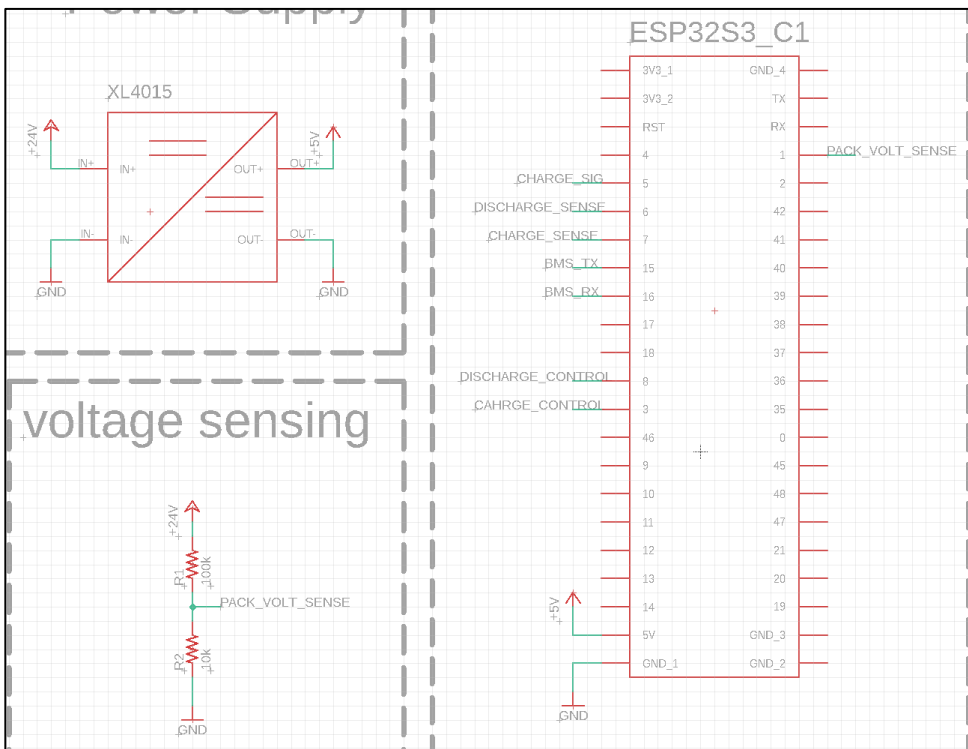


Figure 3.14: The Schematics Diagram of the prototype

### 3.7 Flowchart of the Battery Management System Prototype

Figure 3.15 presents a flowchart detailing the operational sequence and logic of the BMS prototype. This visual representation offers an insightful overview of how the various components and functions of the system interact and operate cohesively to manage and safeguard the battery.

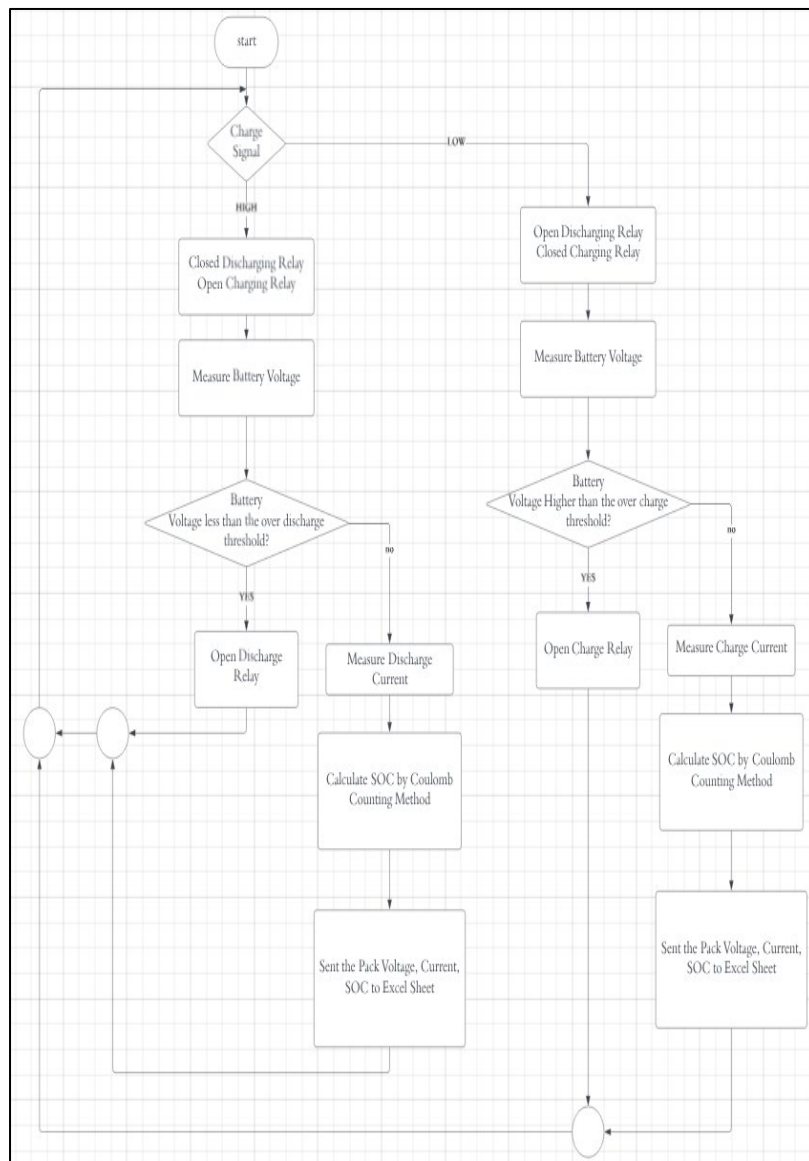


Figure 3.15: The Flowchart of the Control of the Battery Management System.

### 3.8 Data Recording

To facilitate the clear recording of data, including current, battery pack voltage, and SoC from the microcontroller, the Parallax Data Acquisition (PLX-DAQ)

software was employed. This software streamlines the process of systematically storing the data in Microsoft Excel, ensuring that the collected information is organized and easily accessible for analysis and monitoring.

### 3.9 Cost of Building the Battery Management System

Table 3.1 provides a comprehensive list of components along with their corresponding prices. It is worth noting that certain components, such as resistors, bolts, and brass inserts, were excluded from this list as they were sourced from recycled or scrap materials, and therefore did not incur additional costs.

Table 3.1: The BOM list and the Total Price for One Unit of Battery Management System.

No	Item	Price per Unit (RM)	Quantity	Total Price (RM)
1	ESP32S3	18.24	1	18.24
2	7S BMS	9.15	1	9.15
3	INA169	18.2	2	36.4
4	18650 Lithium Ion Battery	9.8	7	68.6
5	Double channel relay module	5.6	1	5.6
			TOTAL	137.99

### 3.10 Gantt Chart

Figures 3.16 and 3.17 show the Gantt chart of the FYP. It outlines the project activities and the respective planned completion dates for the project. For the FYP Part 1, the primary activities include problem identification, extensive literature review, and the selection of suitable components for the BMS prototype.

As for the FYP Part 2, the key activities encompass the construction of the prototype, rigorous testing, and necessary modifications to address unexpected challenges or changes in circumstances. One example of such an adaptation is when the Daly BMS fails to read low current, prompting the need for adjustments and problem-solving in real-time.

no	Project Activities	Planned complete	w1	w2	w3	w4	w5	w6	w7	w8	w9	w10	w11	w12	w13	w14	w15	w16
1	Identify the problem and project planing	9/2/2023	■	■														
2	Conduct Literature Review of the battery management system	26/4/2023		■	■	■	■	■	■	■	■	■	■	■	■			
3	identify the suitable sensors and electronic needed for the prototype	26/4/2023			■	■	■	■	■	■	■	■	■	■	■			
4	progress report writing and presentation	2/5/2023			■	■	■	■	■	■	■	■	■	■	■	■		
5	Circuit Design for the Prototype	19/5/2023															■	■
6	Design the Lithium Ion battery Pack for testing purpose	19/5/2023															■	■

Figure 3.16: The Gantt Chart of FYP1.

no	Project Activities	Planned com	w1	w2	w3	w4	w5	w6	w7	w8	w9	w10	w11	w12	w13	w14	w15	w16
1	construct the battery pack and testing the daly bms	7/7/2023	■	■	■													
2	build the BMS prototype	25/8/2023		■	■	■	■	■	■	■	■	■						
3	Identify the problem of the battery pack and redesign the casing	18/8/2023								■	■							
4	identify the problem of the daly bms and find the current sensor	18/8/2023								■	■							
5	test the functionality of the BMS prototype	15/9/2023											■	■	■			
6	Report Writing and Presentation preparation	17/9/2023												■	■	■		
7	FYP Poster Design and submission	4/9/2023												■				

Figure 3.17: The Gantt Chart of FYP.

### 3.11 Summary

In summary, the final prototype of the battery management system will comprise several key components, including a single 7S battery management system board, two INA169 current sensors, a voltage divider utilized as a voltage sensor, an ESP32S3 microcontroller, and a custom-made 7S lithium-ion battery pack. Data collection will be facilitated by the PLX-DAQ software, with the collected data systematically stored in a Microsoft Excel Sheet for analysis and monitoring.

## CHAPTER 4

### RESULTS AND DISCUSSION

#### 4.1 Introduction

In this chapter, the implementation of the Battery Management System prototype would be delved into. Following the implementation, we will assess the performance of the Battery Management System in safeguarding the 7S lithium battery pack.

#### 4.2 Hardware Implementation

The BMS can be divided into two integral parts. First, there is the 7S lithium-ion battery pack, which is connected in series without the need for soldering. Next, there is the BMS prototype, responsible for executing the functions as designed. These two components work in tandem to ensure the proper management and protection of the battery pack.

##### 4.2.1 7S Lithium-ion Battery Pack

The Lithium-Ion Battery Pack created for the BMS was constructed using a solderless method. Typically, lithium-ion battery packs are assembled by spot welding the battery cells to nickel strips. However, this conventional approach can make it challenging to replace individual cells in the battery pack if any of them malfunction and need to be replaced.

In contrast, the battery pack developed in this project employs a solderless method for assembly. This innovative approach offers the advantage of flexibility, allowing for the easy replacement of individual cells in the event of malfunctions or issues, enhancing the overall maintenance and longevity of the battery pack.

Figure 4.1 illustrates the 7S lithium-ion battery pack, which is connected to the Smart Daly BMS. Following the soldering of the battery balance cable to the juncture where two cells are in series, it is crucial to verify the voltage at the cable connector using a multi-meter. This step ensures that

the potential difference between the points aligns with the voltage of a single cell in the lithium-ion battery.

Subsequently, the connector can be inserted into the balancing port of the Daly BMS, followed by the attachment of the Bluetooth module to the BMS. This process establishes the necessary connections for monitoring and managing the battery pack effectively.

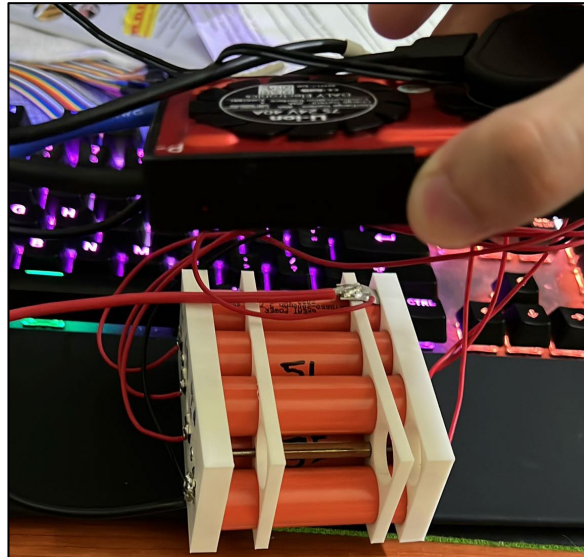


Figure 4.1: The 7S Lithium Battery Pack with Smart Daly BMS.

In Figure 4.2, the depicted app serves as a tool to verify the correct connection of the battery pack to the BMS. Additionally, it provides access to critical data concerning the battery pack's status, including total voltage, SoC, remaining capacity, and even the individual cell voltages within the battery. This app plays a crucial role in monitoring and ensuring the proper functioning of the BMS.



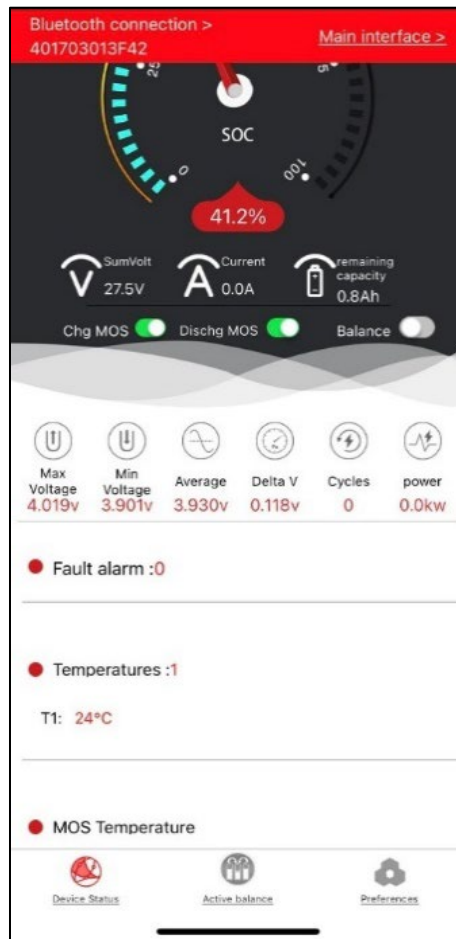


Figure 4.2: The Mobile Phone App of the Daly BMS.

However, during the development process, the Smart Daly BMS encountered certain issues that rendered it unusable. Due to time constraints, a decision was made to replace it with an alternative solution. As a result, modifications were made to the hardware of the BMS as shown in Figures 4.3 and Figures 4.4 in order to adapt to and overcome the challenges that were encountered during the development process.

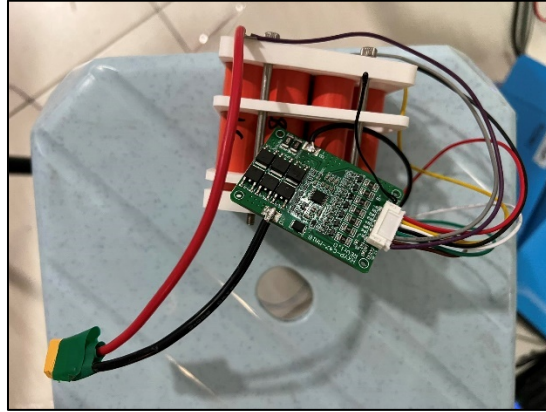


Figure 4.3: The Assembled 7S Lithium-ion Battery Pack with Another BMS.

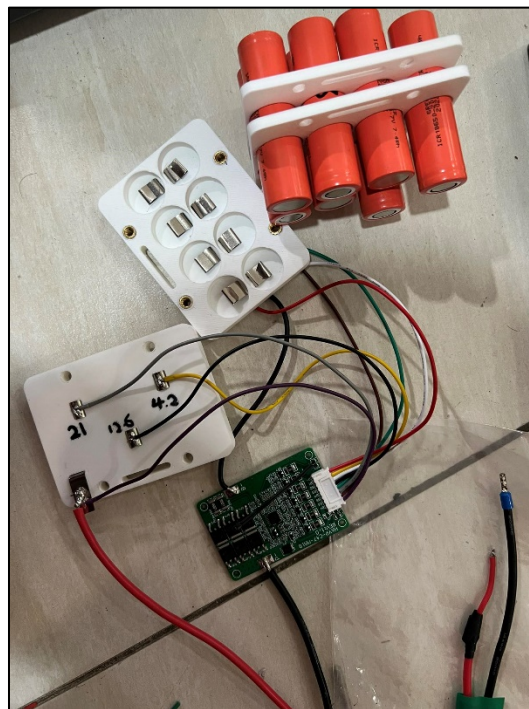


Figure 4.4: The Disassembled 7S Lithium-ion Battery Pack.

#### 4.2.2 Battery Management System Component Specifications

Figure 4.5 shows the electronic components meticulously soldered onto the prototyping board to establish secure electrical connections. This step was crucial in eliminating potential malfunctions of the prototype caused by loose wiring connections.

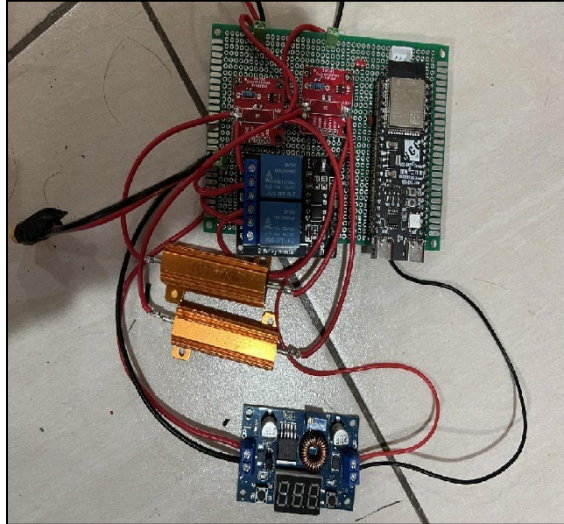


Figure 4.5: The Hardware of the Battery Management System Prototype.

Within the setup, two INA169 shunt current monitor modules, each equipped with a  $0.5\Omega$  shunt resistor, were employed as shown in Figures 4.6 and 4.7. Notably, a modification worth highlighting pertains to the components enclosed in boxes, which represent the  $1k\Omega$  load resistors. These modifications and components are integral to the system's functionality and performance.

Following this, the ESP32S3 microcontroller was incorporated into the BMS to execute the control algorithm and facilitate the transmission of processed data to the computer for data recording. Additionally, a voltage divider circuit was implemented to accurately measure the voltage of the battery pack. These components collectively contribute to the efficient operation of the Battery Management System.

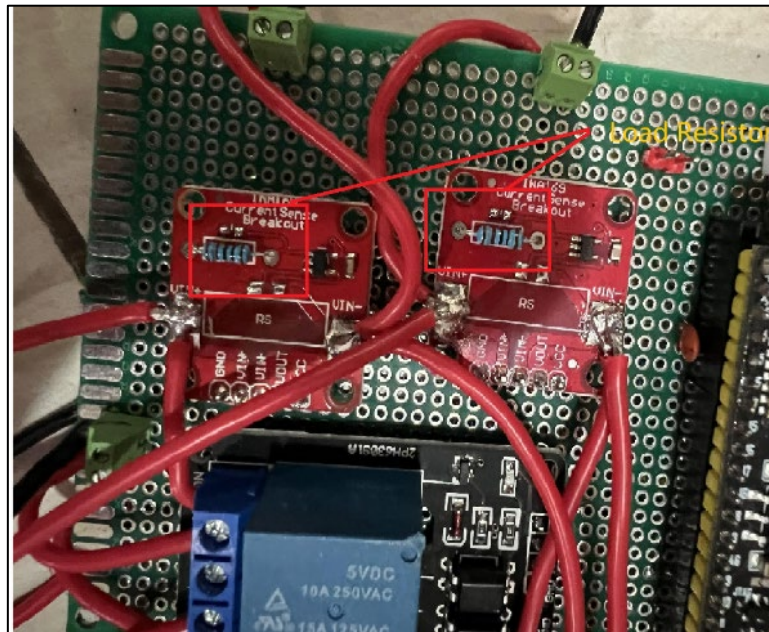


Figure 4.6: The INA169 Shunt Current Monitor Module being Implemented.

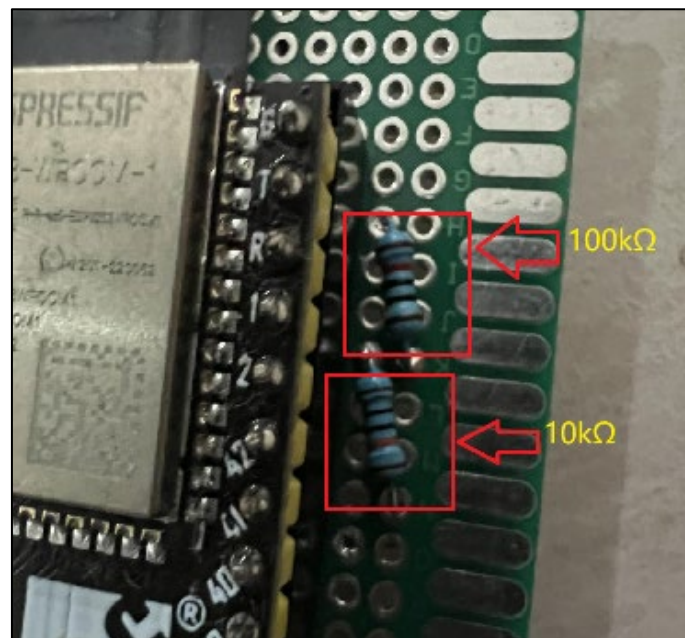


Figure 4.7: The Voltage Sensor of the Battery Management System.

Next, Figure 4.8 shows the relay module used in the BMS. It plays a pivotal role in managing the direction of current within the battery pack. When one of the channels is closed, forming a complete circuit, another channel is opened to ensure that the current flows in only one direction at a time. This control mechanism is essential for maintaining the desired current flow and preventing unwanted electrical feedback or reverse current.

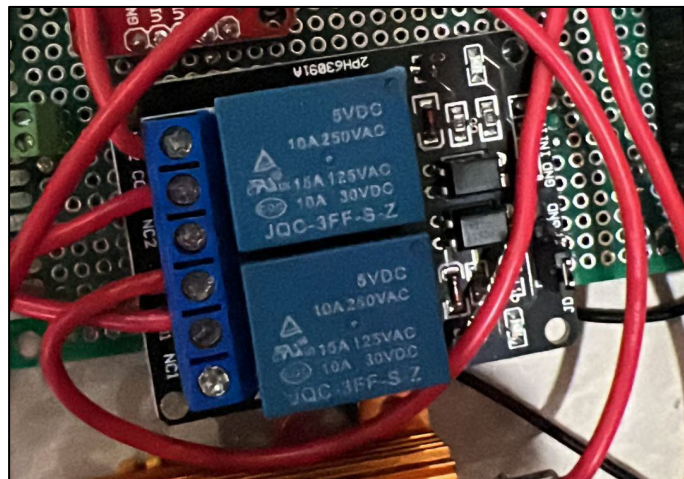


Figure 4.8: The Double Channel Relay Module.

Lastly, the DC-DC converter used in the BMS is shown in Figure 4.9. The primary function of the DC-DC buck converter is to supply power to both the relay module and the microcontroller. The input for the buck converter is derived directly from the battery pack. The output voltage of the buck converter is adjusted to approximately 5V, as this voltage level is necessary to trigger and operate the relay module effectively. This setup ensures that both components receive the appropriate voltage to function correctly.

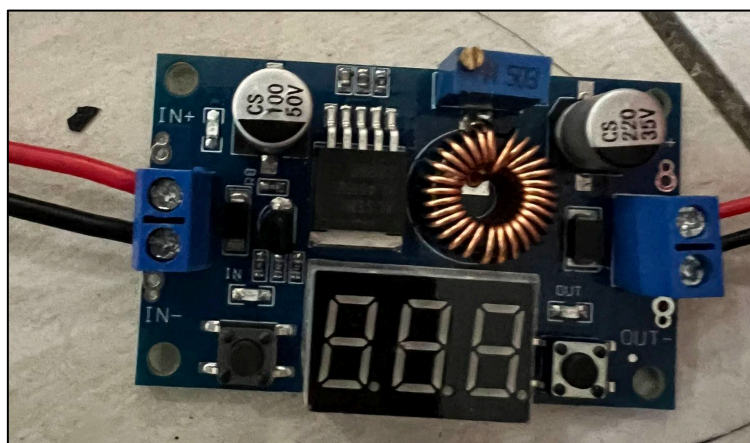


Figure 4.9: The DC-DC Buck Converter being Implemented.

### 4.3 Software Implementation

Moving on, in terms of software implementation, the BMS prototype's software was developed using the Arduino IDE. Subsequently, the code was

loaded or flashed into the microcontroller, allowing it to execute the programmed instructions and functions as designed. This approach provides a user-friendly and versatile platform for developing and deploying the software for the BMS.

#### **4.4 Implementation Issues and Challenges**

During the implementation process, several challenges and issues were encountered. To address these, various solutions and modifications were applied to the prototype in order to overcome these challenges and ensure the successful development and operation of the BMS.

##### **4.4.1 Sensitivity of the Current Sensor Inside Daly Smart Battery Management System**

The initial plan for the BMS involved the implementation of the Smart Daly BMS to perform data acquisition, collecting crucial information such as charging and discharging current and battery pack voltage. However, as the development process unfolded, it became evident that the current sensor within the Daly BMS was unable to detect charging or discharging currents below or around one ampere as shown in Figures 4.10 and 4.11. This limitation not only affected the accuracy of the SoC estimation provided by the Daly BMS but also rendered the SoC data unreliable when the battery was subjected to charging or discharging currents below one ampere. This issue prompted the need for an alternative solution to address the shortcomings of the initial plan.

As depicted in the stated figures, the charging current was measured at 1.02 A. However, the data displayed on the Daly BMS app indicated that no current was detected. To address this issue and rectify the problem of current sensing, the design incorporated two current sensors as a solution. This adjustment aimed to ensure accurate and reliable current measurements, resolving the earlier issue of undetected currents.

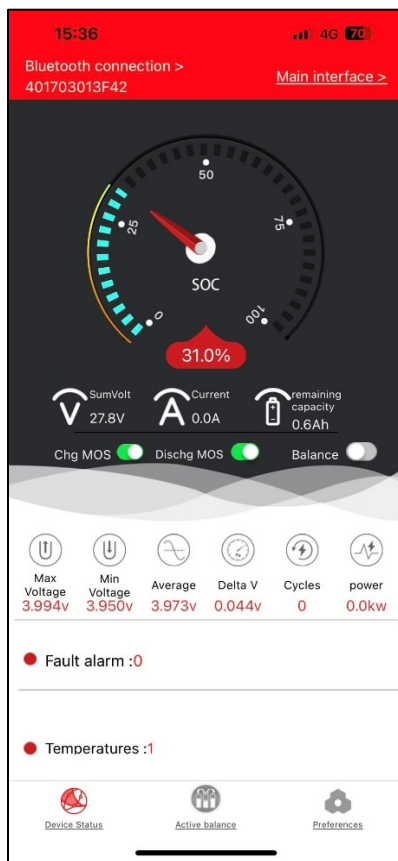


Figure 4.10: The GUI of the Daly BMS during Charging Current Around One Ampere.

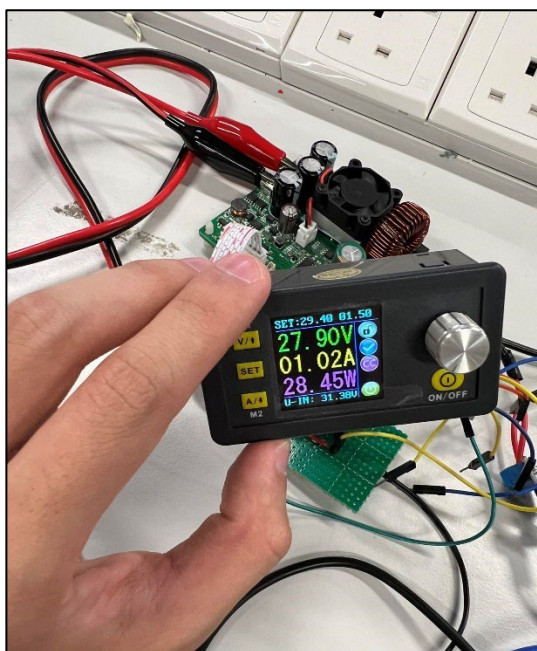


Figure 4.11: The Charging Current Output by the Charger.

#### **4.4.2 State of Charge of the Battery Management System**

The SoC of the battery is a critical parameter that informs users about the percentage of remaining battery capacity. In this design, the algorithm of the microcontroller incorporates the coulomb counting method to estimate the SoC of the lithium-ion battery pack.

However, a challenge with this method is that it requires knowledge of the initial state of charge of the battery before the microcontroller can accurately perform coulomb counting. To address this issue, a solution was implemented: the battery pack needed to be disassembled, and the individual battery cells were fully charged before reassembling the battery pack. This initial SoC was then programmed as 100% in the microcontroller's software.

One limitation of this solution is that if the microcontroller is reset, the SoC of the battery would reset to 100%, and the battery pack would need to be disassembled and the cells fully charged again. This process would need to be repeated each time the microcontroller is reset, which could be seen as a drawback in terms of convenience and user-friendliness.

#### **4.4.3 Tolerance of the Resistor**

When implementing the voltage sensor using a voltage divider, it is crucial to consider the actual resistance values of the resistors used. Resistors may have slightly different values compared to their typical or nominal values due to manufacturing tolerances. Therefore, relying on the typical resistance values in the algorithm for calculating the pack voltage measured by the sensor may lead to inaccuracies.

To address this issue, the actual resistance values of the resistors need to be measured using a digital multi-meter, and these measured values should be applied in the voltage sensing algorithm. In Figure 4.12, it appears that the actual resistance values of the voltage divider have been incorporated into the software to ensure accurate voltage measurements, accounting for the variations in resistor values.



```
const float R1 = 94.0; // resistance in k ohm  
const float R2 = 9.9; // resistance in k ohm
```

Figure 4.12: The Actual Resistance of R1 and R2 Measured.

## 4.5 System Evaluation and Discussion

The proposed BMS underwent an evaluation to assess its functionality, specifically focusing on the functions that were implemented within it. These functions included current sensing, voltage sensing, and SoC estimation using the coulomb counting method. This evaluation aimed to verify the system's performance and ensure that it accurately measured and estimated these critical parameters related to battery management.

### 4.5.1 Current Sensing

According to Figure 4.13, the discharging current supplied to the electronic load tester is recorded at 0.344A. Simultaneously, the voltage measured across the shunt resistor of the current sensor registers at 0.172V. These measurements are crucial for accurately monitoring the battery's performance and ensuring that the current sensing function is functioning as intended in the BMS.

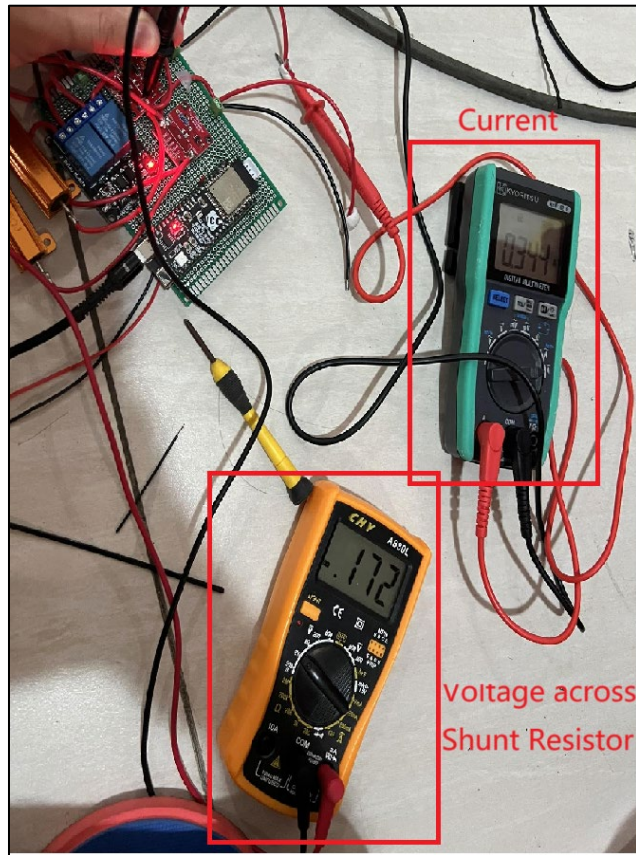


Figure 4.13: The Discharging Current and Voltage Across Shunt Resistor.

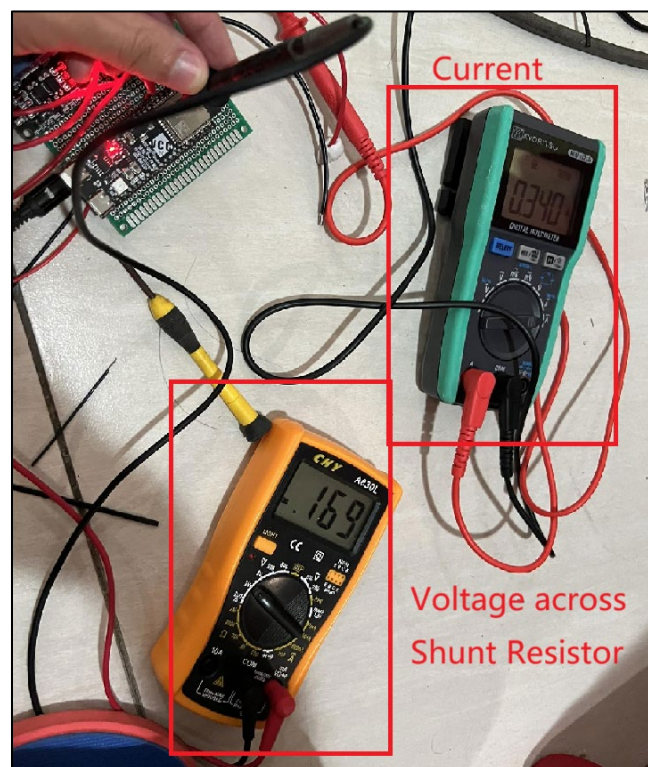


Figure 4.14: The Discharging Current and Voltage Across Shunt Resistor.

Following the adjustment to the discharging current, the current was recorded at 0.340A, while the voltage measured across the shunt resistor stood at 0.169V. These precise measurements were documented and included in Table 4.1 for reference and analysis, ensuring accurate monitoring and assessment of the BMS's performance.

Table 4.1: The Discharging Current and the Respective Voltage

<b>Test</b>	<b>Discharging current, A</b>	<b>Voltage across shunt resistor (measured), V</b>	<b>Voltage across shunt resistor (calculated)</b>	<b>Percentage Error, %</b>
1	0.340	0.169	0.170	0.59
2	0.344	0.172	0.172	0.00

By applying Ohm's Law, which states  $V = IR$ , where  $V$  represents voltage,  $I$  represents current, and  $R$  represents resistance, we can calculate the expected voltage across the shunt resistor. With a known shunt resistance of  $0.5\Omega$  and the measured discharging current, we can substitute the current value into the formula to calculate the expected voltage.

To assess the accuracy of the current sensor, the percentage error between the calculated voltage and the measured voltage across the shunt resistor was determined using Equation (4.1). According to the results presented in Table 4.1, the percentage error for the current sensor was found to be less than 1%. This low percentage error indicates that the current sensing function of the BMS is highly accurate and reliable.

#### 4.5.2 Voltage Sensing

During the implementation process, the voltage sensor successfully measured the battery pack voltage. Multiple trials were conducted as shown from Figure 4.14 to 4.19 to compare the voltage readings obtained from the voltage sensor with those obtained using a multi-meter. The results of these trials were summarized in Table 4.2.

Following the data collection, the percentage errors of the voltage sensor were calculated. These calculations aimed to assess the accuracy of the

voltage sensing function within the BMS and provide insights into its performance.

1.680000	26.38	92.99
1.670000	26.38	92.97
1.690000	26.37	92.95
1.670000	26.37	92.92
1.680000	26.37	92.9
1.680000	26.37	92.88
1.680000	26.37	92.85
1.680000	26.36	92.83
1.680000	26.36	92.81
1.670000	26.35	92.78
1.680000	26.34	92.76
1.690000	26.35	92.74
1.680000	26.35	92.71
1.680000	26.34	92.69

Figure 4.15: The Voltage Measured by the Voltage Sensor (Trial 1).



Figure 4.16: The Voltage Measured by the Multi-meter (Trial 1).

C	D	E
<b>Current</b>	<b>Voltage</b>	<b>SocDATA</b>
1.690000	26.22	91.52
1.680000	26.21	91.5
1.690000	26.18	91.47
1.690000	26.18	91.45
1.690000	26.17	91.43
1.680000	26.18	91.4
1.680000	26.18	91.38
1.700000	26.17	91.36
1.690000	26.17	91.33
1.680000	26.17	91.31
1.690000	26.17	91.29
1.690000	26.17	91.26

Figure 4.17: The Voltage Measured by the Voltage Sensor (Trial 2).

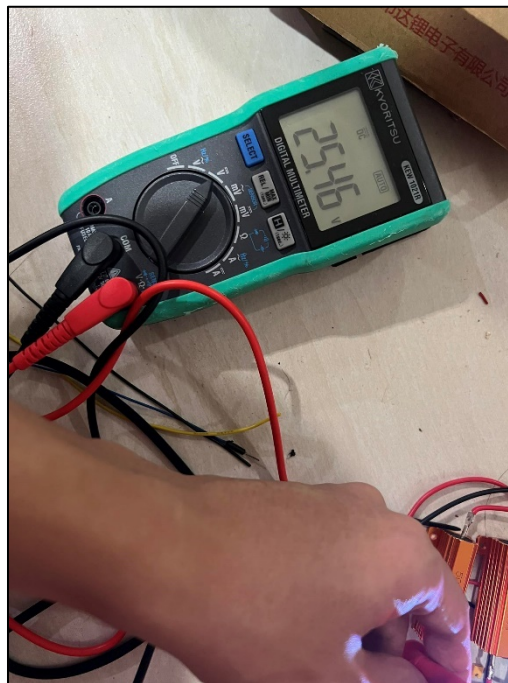


Figure 4.18: The Voltage Measured by the Multi-meter (Trial 2).

1.700000	25.76	87.61
1.700000	25.77	87.59
1.710000	25.76	87.57
1.690000	25.76	87.54
1.690000	25.76	87.52
1.700000	25.76	87.49
1.680000	25.76	87.47
1.690000	25.76	87.45
1.690000	25.75	87.42
1.700000	25.75	87.4
1.700000	25.75	87.38
1.680000	25.74	87.35
1.690000	25.73	87.33
1.690000	25.73	87.31
1.690000	25.73	87.28
1.690000	25.72	87.26
1.680000	25.72	87.24
1.680000	25.72	87.21
1.680000	25.72	87.19

Figure 4.19: The Voltage Measured by the Voltage Sensor (Trial 3).



Figure 4.20: The Voltage Measured by the Multi-meter (Trial 3).

Table 4.2: The Trials of Voltage Measurement using Multi-meter and Voltage Sensor

Test	Voltage measured by Voltage Sensor, V	Voltage Measured with Multi-meter, V	Percentage Error, %
1	26.34	25.65	2.69
2	26.17	25.46	2.79
3	25.72	25.00	2.88

#### 4.5.3 Discharging Process of the Battery Pack

A constant discharging current of 1.83 A as shown in Figure 4.20 was applied by connecting the battery pack to the electronic load tester. Subsequently, the battery pack was allowed to discharge continuously until the relay module opened the circuit. This process was likely part of the testing and evaluation procedure to determine the battery pack's performance and behaviour under such conditions.

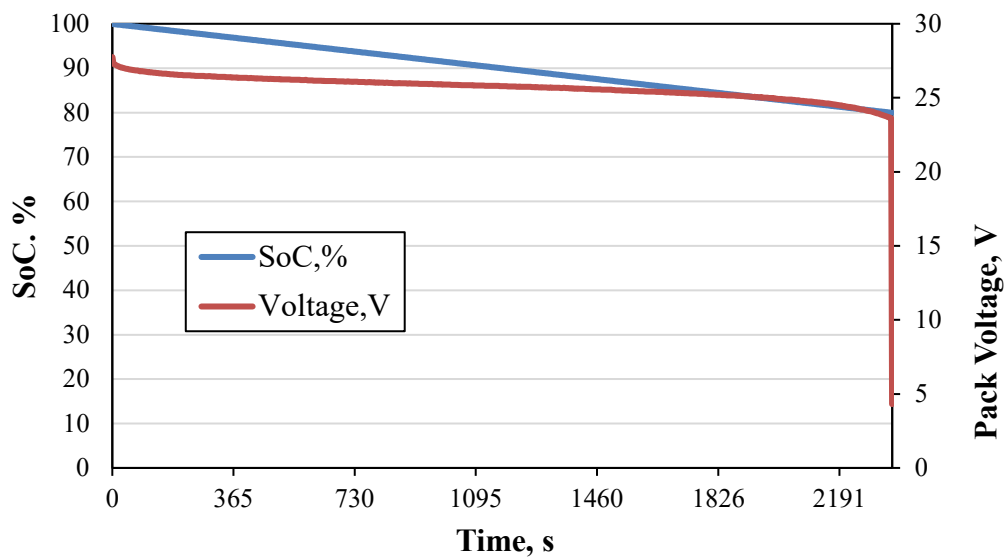


Figure 4.21: The SOC and Pack Voltage Versus Time Curve.

#### 4.5.4 Discharge and Charging of the Battery Pack

Figure 4.21 illustrates the discharging and charging process of the battery pack. During the discharging phase, the battery pack was discharged at a constant current of 1.67A for a duration of 1203 seconds. Subsequently, during the

charging phase, the battery pack was charged with a constant current of 0.79A for a period of 1254 seconds. These details provide insight into the specific current levels and time durations involved in the battery's discharging and charging cycles, which are critical parameters for evaluating battery performance and behaviour.

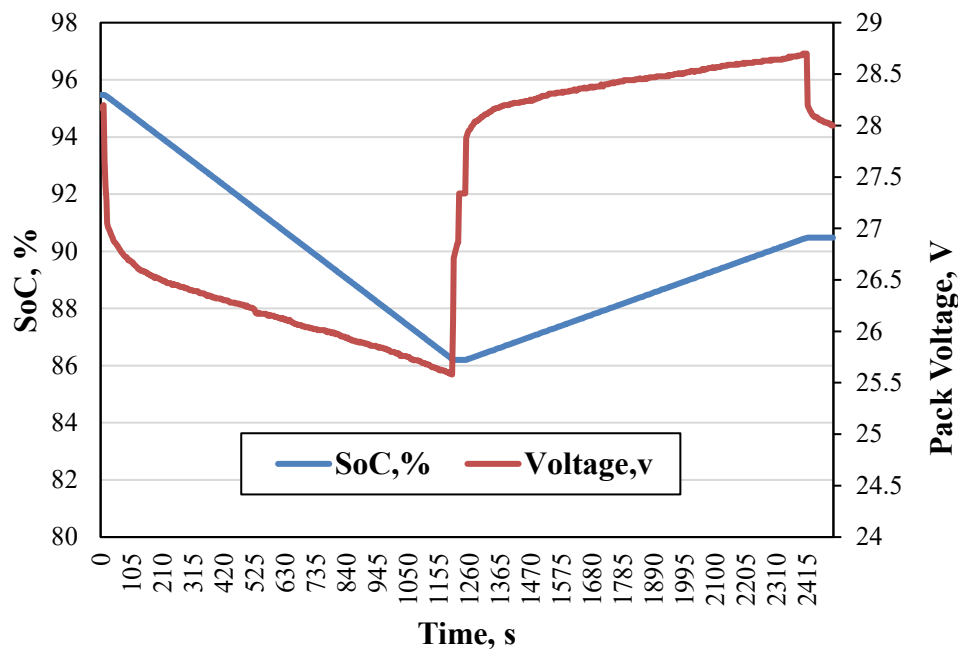


Figure 4.22: Discharging and Charging Voltage and SOC of the Battery Pack.

#### 4.6 Summary

During the implementation process, various challenges and issues were encountered, but each problem was met with a well-thought-out solution. As a result, the BMS prototype was successfully configured to perform its designated tasks. The BMS prototype is now capable of accurately measuring the charging and discharging currents of the battery pack. Furthermore, the implemented voltage sensor effectively monitors the voltage of the battery pack. Additionally, the SoC estimation, achieved through the coulomb counting method, accurately calculates the SoC of the battery pack during both charging and discharging processes. These achievements demonstrate the successful development and functionality of the BMS prototype.



## CHAPTER 5

### CONCLUSIONS AND RECOMMENDATIONS

#### 5.1 Conclusions

In conclusion, the development of the BMS has been successful, achieving its intended functionalities. The system is now capable of accurately measuring the current, pack voltage, and SoC of the battery pack.

The INA169 current sensor has demonstrated good accuracy in measuring current, exhibiting low percentage errors in its measurements. Additionally, the voltage divider circuit, when configured with the appropriate resistance values, has proven to be a suitable and accurate voltage sensor.

However, it is important to note that the coulomb counting method used for SoC estimation relies on knowing the initial SoC of the battery. This presents a limitation in cases where the microcontroller is reset due to power brownouts or other uncertainties, potentially causing inaccuracies in SoC calculations. This limitation should be considered when using the battery management system in practical applications.

The development of the BMS has successfully achieved its intended objectives, aligning with the overarching aim of monitoring and controlling battery parameters during the charging and discharging processes of AGV, specifically those designed and developed at UTAR. The objectives set forth for this project have been met as follows:

- **Sensor and Electronics Selection:** The project identified and selected the appropriate sensors and electronic components necessary for the BMS development, ensuring the system's compatibility and accuracy.
- **BMS Prototype Development:** The core objective of creating a functional BMS prototype for AGV applications was successfully realized, encompassing critical functionalities such as current measurement, voltage sensing, and SoC estimation.

- **Performance Validation:** The performance of the developed BMS was rigorously validated, affirming its capabilities in accurately measuring current, monitoring pack voltage, and estimating SOC, while also addressing potential challenges such as current sensing accuracy and initial SOC knowledge.

By achieving these objectives, the project has contributed to advancing the field of battery management for AGVs, enhancing the reliability and efficiency of these systems in real-world applications. It is worth to highlight that this FYP has won the 2022/2023 Innovate Malaysia Design Competition Champion title under the track of IR4.0 in part with another two FYPs whose topic was targeted on the battery pack charging strategies and the current limit solution using hybrid energy storage system of battery and supercapacitor. The work covered in the report containing the BMS where it integrates the features and functions of the other two systems into the AGV's battery pack solution.

## **5.2 Recommendations for Future Work**

In light of the challenges faced during this project, several important recommendations for future work have emerged, which have the potential to further enhance the BMS prototype:

1. **EEPROM Integration for SOC Persistence:** One significant advancement is the utilization of the microcontroller's built-in electrically erasable programmable read-only memory (EEPROM) to address the issue of SOC data loss during accidental microcontroller resets. To expand on this recommendation, future work could focus on developing a robust algorithm for SOC data management within the EEPROM. Additionally, the implementation of fail-safe mechanisms to safeguard against power outages and ensure uninterrupted data retention would be valuable.

2. Custom PCB Design: To optimize the BMS prototype for practical use and commercial applications, the transition from pre-assembled electronic modules to a custom printed circuit board (PCB) design is highly advisable. Elaborating on this, future efforts could involve the design and fabrication of a compact and tailored PCB layout that not only reduces the size of the prototype but also enhances its overall safety and reliability. Further exploration of surface-mounted components as opposed to through-hole counterparts should be considered to minimize space requirements and improve component integration.
3. Enhanced Sensor Integration: Building on the concept of miniaturization, future work could delve into the integration of more advanced and compact sensor technologies, optimizing the BMS's overall efficiency and footprint. Additionally, research into sensor redundancy and data validation techniques may contribute to the development of a more robust and accurate monitoring system.
4. Real-time Data Logging and Analysis: For comprehensive battery management, future iterations of the BMS could incorporate real-time data logging and analysis capabilities. This could involve the integration of data communication protocols such as Bluetooth or Wi-Fi, enabling remote monitoring and data retrieval. Moreover, the development of user-friendly software interfaces for data visualization and analysis would be a valuable addition, facilitating informed decision-making regarding battery maintenance and performance optimization.
5. Safety and Reliability Testing: Extensive safety and reliability testing should be a focal point of future work. This entails subjecting the BMS to various stress tests, environmental conditions, and operational scenarios to ensure its robustness and durability in real-world AGV applications.

By addressing these recommendations in future research and development endeavours, the BMS can be further refined, making it a crucial tool for optimizing the performance, lifespan, and safety of batteries used in AGVs and other applications. These advancements have the potential to significantly impact the field of battery management and contribute to the efficiency and sustainability of AGV systems.

## REFERENCES

- Akarслан, E. and Çinar, S.M., 2022. A Battery Management System Design Including a SOC Estimation Approach for Lead-Acid Batteries. *Journal of Materials and Mechatronics: A*. <https://doi.org/10.55546/jmm.1193510>.
- Bhatt, A., Forsyth, M., Withers, R. and Guoxiu, W., 2017. *Why do I have to charge my new rechargeable batteries before use? - Curious*. [online] Australian Academy of Science. Available at: <<https://www.science.org.au/curious/technology-future/why-do-i-have-charge-my-new-rechargeable-batteries-use>> [Accessed 23 April 2023].
- Cao, J., Schofield, N. and Emadi, A., 2008. Battery balancing methods: A comprehensive review. In: *2008 IEEE Vehicle Power and Propulsion Conference*. pp.1–6. <https://doi.org/10.1109/VPPC.2008.4677669>.
- Ceven, S., Kucukkulahli, E., Albayrak, A. and Bicen, Y., 2021. Development of IoT Based Battery Management System. In: *2nd International Informatics and Software Engineering Conference, IISEC 2021*. Institute of Electrical and Electronics Engineers Inc. pp.1–5. <https://doi.org/10.1109/IISEC54230.2021.9672346>.
- Lakkireddy, G.R. and Mathe, S.E., 2022. A Strategy for Measuring Voltage, Current and Temperature of a Battery Using Linear Optocouplers. *World Electric Vehicle Journal*, 13(12), pp.4–5. <https://doi.org/10.3390/wevj13120225>.
- Lelie, M., Braun, T., Knips, M., Nordmann, H., Ringbeck, F., Zappen, H. and Sauer, D.U., 2018. Battery management system hardware concepts: An overview. *Applied Sciences (Switzerland)*, 8(4), pp.3–3. <https://doi.org/10.3390/app8040534>.
- Li, L., Li, Z., Zhao, J. and Guo, W., 2018. Lithium-ion battery management system for electric vehicles. *International Journal of Performability Engineering*, 14(12), pp.3184–3194. <https://doi.org/10.23940/ijpe.18.12.p28.31843194>.
- Lynch, L., Coleman, J., Newe, T., Walsh, J., Clifford, J. and Toal, D., 2018. Automated Ground Vehicle (AGV) and Sensor Technologies-A Review.
- Maloney, D., 2018. *An E-Bike Battery Pack Without Spot Welding | Hackaday*. [online] Available at: <<https://hackaday.com/2018/07/03/an-e-bike-battery-pack-without-spot-welding/>> [Accessed 17 September 2023].
- Maxim Integrated, n.d. *Precision, High-Side Current-Sense Amplifier*. [online] Available at: <<https://www.analog.com/media/en/technical-documentation/data-sheets/MAX471-MAX472.pdf>> [Accessed 5 October 2023].

Movassagh, K., Raihan, A., Balasingam, B. and Pattipati, K., 2021. A critical look at coulomb counting approach for state of charge estimation in batteries. *Energies*, 14(14), pp.8–8. <https://doi.org/10.3390/en14144074>.

Nizam, M., Maghfiroh, H., Rosadi, R.A. and Kusumaputri, K.D.U., 2019. Design of Battery Management System (BMS) for Lithium Iron Phosphate (LFP) Battery. In: *International Conference on Electric Vehicular Technology (ICEVT)*. IEEE. pp.1–5. <https://doi.org/10.1109/ICEVT48285.2019.8994002>.

Omariba, Z.B., Zhang, L. and Sun, D., 2019. Review of Battery Cell Balancing Methodologies for Optimizing Battery Pack Performance in Electric Vehicles. *IEEE Access*, 7, pp.129335–129352. <https://doi.org/10.1109/ACCESS.2019.2940090>.

Shete, S., Jog, P., Palwalia, D.K. and Kumawat, R.K., n.d. Battery Management System for SOC Estimation of Lithium-Ion Battery in Electric Vehicle: A Review. <https://doi.org/10.1109/ICRAIE52900.2021.9703752>.

Texas Instrument, 2016. *20-Series Battery Management Module Reference Design*. [online] Available at: <<https://www.ti.com/lit/pdf/tiduc43>> [Accessed 5 October 2023].

Wang, J. and Yin, Z., 2021. Overview of key technologies of battery management system. In: *Journal of Physics: Conference Series*. IOP Publishing Ltd. pp.2–5. <https://doi.org/10.1088/1742-6596/2030/1/012009>.

Wang, Y., Tian, J., Sun, Z., Wang, L., Xu, R., Li, M. and Chen, Z., 2020. A comprehensive review of battery modeling and state estimation approaches for advanced battery management systems. *Renewable and Sustainable Energy Reviews*, 131, pp.3–5. <https://doi.org/10.1016/j.rser.2020.110015>.

Winson, 2020. *Hall Effect Base Linear Current Sensor*. [online] Available at: <<http://www.winson.com.tw/uploads/images/WCS1800.pdf>> [Accessed 29 April 2023].

Xing, Y., Ma, E.W.M., Tsui, K.L. and Pecht, M., 2011. Battery management systems in electric and hybrid vehicles. *Energies*, 4(11), pp.1840–1857. <https://doi.org/10.3390/en4111840>.

## APPENDICES

Appendix A: The Code of the Battery Management System Prototype (main).

```
#include "relay_control.h"
#include "current_sensing.h"

#include "WString.h"
#include "HardwareSerial.h"

#include "WiFi.h"

float current = 0.0;
float soc = 0.0;
float pack_voltage = 0.0;
void discharge_battery_record(void);
void charge_battery_record(void);
const int charge_sig = 5;

void setup() {
    // put your setup code here, to run once:
    Serial.begin(9600);
    pinMode(charge_sig, INPUT_PULLUP);
    Serial.println("CLEARSHEET");
    Serial.print("LABEL, TIME, time_elapse, Current, Voltage, Soc");

    relay_init();
    charge_battery(true);
}

void loop() {
    // put your main code here, to run repeatedly:
    //measure_current();
    //the relay module is low to trigger.
    if(digitalRead(charge_sig) == 0){
        discharge_battery(false);
        charge_battery(true);
        charge_battery_record();
    }
    else{
        discharge_battery(true);
        charge_battery(false);
        charge_battery_record();
    }
}

void charge_battery_record(void){
    if(get_voltage() > 28.7){
        charge_battery(false);
    }
}
```

```

    discharge_battery(false);
    charge_flag = false;
}
else {
    current = measure_current(charge_sense);
    soc = coulomb_counting_charging_soc(initial_soc_battery,
current);
    initial_soc_battery = soc;
    pack_voltage = get_voltage();
    Serial.print("DATA, TIME,");
    Serial.print(millis());
    Serial.print(",");
    Serial.print(current);
    Serial.print(",");
    Serial.print(pack_voltage);
    Serial.print(",");
    Serial.print(soc);
    Serial.print(",");
    Serial.println("AUTOSCROLL_20");
}
}
}

void discharge_battery_record(){
    if(get_voltage() < 22.4){
        charge_battery(false);
        discharge_battery(false);
        discharge_flag= false;
    }
    else{
        current = measure_current(discharge_sense);
        soc = coulomb_counting_discharging_soc(initial_soc_battery,
current);
        initial_soc_battery = soc;
        pack_voltage = get_voltage();
        Serial.print("DATA, TIME,");
        Serial.print(millis());
        Serial.print(",");
        Serial.print(current);
        Serial.print(",");
        Serial.print(pack_voltage);
        Serial.print(",");
        Serial.print(soc);
        Serial.print(",");
        Serial.println("AUTOSCROLL_20");
    } }
}
}

```



## Appendix B: The Subfile of the Code (relay\_control.h)

```

#ifndef RELAY_CONTROL_H
#define RELAY_CONTROL_H

extern const uint8_t discharge_control;
extern const uint8_t charge_control;

void relay_init(void);
void charge_battery(bool status);
void discharge_battery(bool status);

#endif

```

## Appendix C: The Subfile of the Code (relay\_control.cpp)

```

#include "esp32-hal-gpio.h"
#include "relay_control.h"
#include "Arduino.h"

const uint8_t discharge_control = 8; //IN2
const uint8_t charge_control = 3; //IN1

//const uint8_t charge_sig =
void relay_init(){
    pinMode(discharge_control, OUTPUT);
    pinMode(charge_control, OUTPUT);
    digitalWrite(discharge_control, HIGH);
    digitalWrite(charge_control, HIGH);
}

//the function to charge the battery by closing the relay between
//charger and the battery.
void charge_battery(bool status){
    if(status == true){
        digitalWrite(charge_control, LOW);
    }
    else{
        digitalWrite(charge_control, HIGH);
    }
}

//the function to discharge the battery by closing the relay
//between load and the battery.
void discharge_battery(bool status){
    if(status == true){
        digitalWrite(discharge_control, LOW);
    }
    else{
        digitalWrite(discharge_control, HIGH);
    }
}

```

```
}
}
```

#### Appendix D: The Subfile of the Code (current\_sensing.h)

```
#ifndef CURRENT_SENSING_H
#define CURRENT_SENSING_H

extern const int charge_sense; // pin for the charge current
sensing
extern const int discharge_sense; // pin for the
discharge current sensing
extern float initial_soc_battery;

void current_sensor_init(void);
float measure_current(int current_sense_pin);
float measure_current_milli(int current_sense_pin, int interval);
float coulomb_counting_charging_soc(float soc_t_minus_one, float
measured_current);
float coulomb_counting_discharging_soc(float soc_t_minus_one,
float measured_current);
float get_voltage(void);
#endif
```

#### Appendix E: The Subfile of the Code (current\_sensing.cpp)

```
#include "esp32-hal.h"
#include "esp32-hal-adc.h"
#include "current_sensing.h"
#include "Arduino.h"
#include "Statistic.h"

const int charge_sense = 7;
const int discharge_sense = 6;
const int voltage_sense = 1;
const float shunt_resistance = 0.5;
const float Vref = 3.3; // the reference voltage of the adc.
const int adc_resolution = 4096;
const float voltage_offset = 1.72;
float sensor_value;

unsigned long previous_millis = 0;
unsigned long current_millis;

const float battery_cap_AH = 2.0;

float initial_soc_battery = 100.0;
```

```

const float R1 = 94.0; // resistance in k ohm
const float R2 = 9.9; // resistance in k ohm

float measure_current(int current_sense_pin){

    float averaged_current = 0.0;
    for(int x = 0; x<=1000;x++){
        sensor_value += analogRead(current_sense_pin);
        delay(1);
        //delay(50);
    }
    sensor_value/=1000;
    //Serial.println(sensor_value);
    sensor_value = (sensor_value * Vref) / 4096;
    float current = sensor_value / 0.5;
    //current[0].add(current);
    //Serial.println(current);
    return current;
}

float coulomb_counting_charging_soc(float soc_t_minus_one, float
measured_current){
    float measured_AH = measured_current / 3600;
    float measured_soc = (measured_AH / battery_cap_AH) * 100.0; //
the measured soc in %
    float total_soc = soc_t_minus_one + measured_soc;
    return total_soc;
}

float coulomb_counting_discharging_soc(float soc_t_minus_one,
float measured_current){
    float measured_AH = measured_current / 3600;
    float measured_soc = (measured_AH / battery_cap_AH) * 100.0; //
the measured soc in %
    float total_soc = soc_t_minus_one - measured_soc;
    return total_soc;
}

float get_voltage(){
    float voltage_ratio = R2/(R1+R2);
    float average_Vout = 0.0;
    for(int x = 0; x<=1000;x++){
        average_Vout += analogRead(voltage_sense);
        delay(1);
    }
    average_Vout/=1000;
    average_Vout = (average_Vout * Vref) / 4096;
}

```

```

float sensed_voltage = average_Vout / voltage_ratio;
return (sensed_voltage + voltage_offset);
}

```

## Appendix F: Datasheet of INA169 Shunt Current Monitor

**TEXAS  
INSTRUMENTS**

**INA139, INA169**  
SBOS181F – DECEMBER 2000 – REVISED FEBRUARY 2017

### INA1x9 High-Side Measurement Current Shunt Monitor

#### 1 Features

- Complete Unipolar High-Side Current Measurement Circuit
- Wide Supply and Common-Mode Range
- INA139: 2.7 V to 40 V
- INA169: 2.7 V to 60 V
- Independent Supply and Input Common-Mode Voltages
- Single Resistor Gain Set
- Low Quiescent Current: 60  $\mu$ A (Typical)
- 5-Pin, SOT-23 Packages

#### 2 Applications

- Current Shunt Measurement:
  - Automotive, Telephone, Computers
- Portable and Battery-Backup Systems
- Battery Chargers
- Power Management
- Cell Phones
- Precision Current Source

#### 3 Description

The INA139 and INA169 are high-side, unipolar, current shunt monitors. Wide input common-mode voltage range, high-speed, low quiescent current, and tiny SOT-23 packaging enable use in a variety of applications.

Input common-mode and power-supply voltages are independent and can range from 2.7 V to 40 V for the INA139 and 2.7 V to 60 V for the INA169. Quiescent current is only 60  $\mu$ A, which permits connecting the power supply to either side of the current measurement shunt with minimal error.

The device converts a differential input voltage to a current output. This current is converted back to a voltage with an external load resistor that sets any gain from 1 to over 100. Although designed for current shunt measurement, the circuit invites creative applications in measurement and level shifting.

Both the INA139 and INA169 are available in 5-pin SOT-23 packages. The INA139 device is specified for the  $-40^{\circ}\text{C}$  to  $+125^{\circ}\text{C}$  temperature range, and the INA169 is specified from  $-40^{\circ}\text{C}$  to  $+85^{\circ}\text{C}$ .

**Device Information<sup>(1)</sup>**

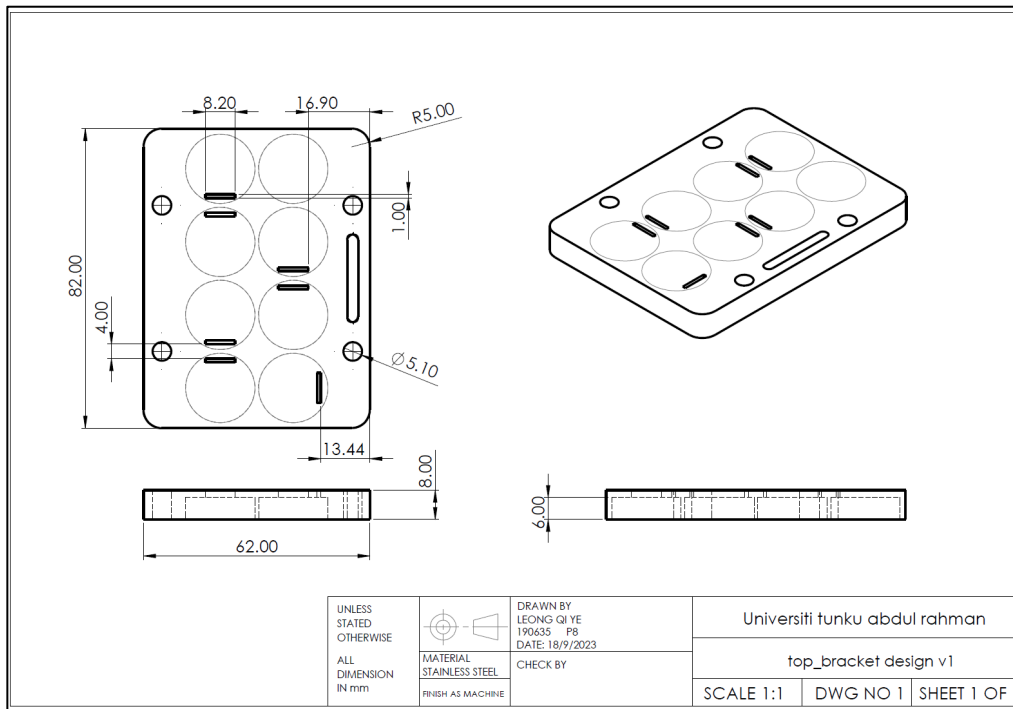
PART NUMBER	PACKAGE	BODY SIZE (NOM)
INA139	SOT-23 (5)	2.90 mm $\times$ 1.60 mm
INA169		

(1) For all available packages, see the orderable addendum at the end of the data sheet.

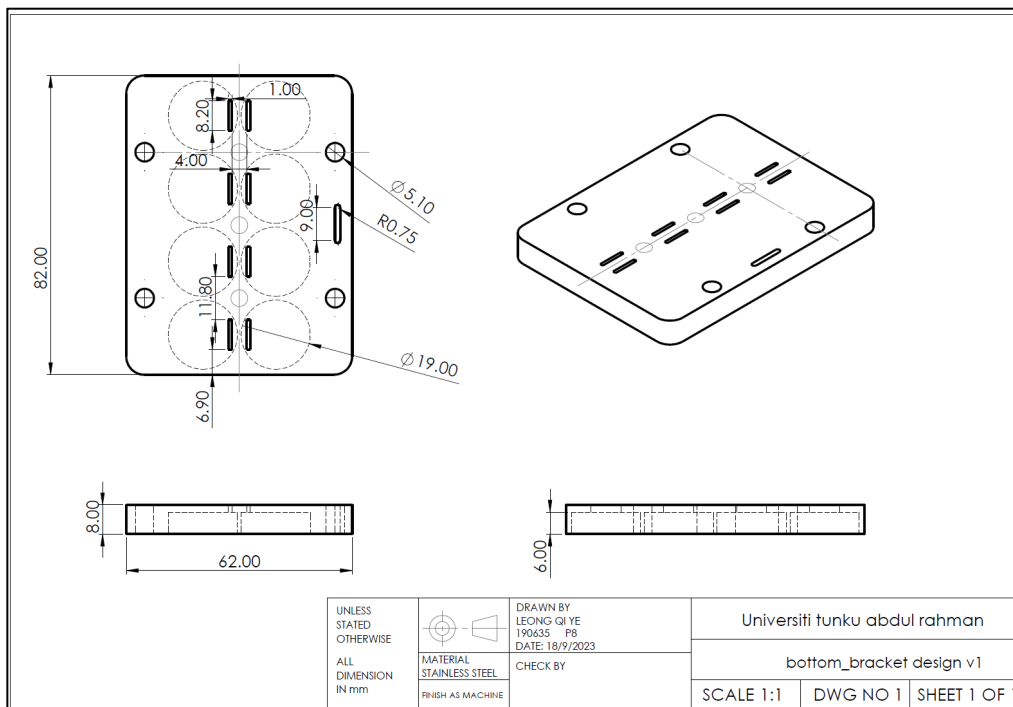
**Typical Application Circuit**

Copyright © 2017, Texas Instruments Incorporated

Appendix G: The Drawing of Battery Casing (Top Bracket)



Appendix H: The Drawing of Battery Casing (Bottom Bracket)



Appendix I: The Drawing of Battery Casing (8S Bracket but can Fit 7S also)

